AMERICAN METEOROLOGICAL SOCIETY

Journal of Physical Oceanography

EARLY ONLINE RELEASE

The DOI for this manuscript is doi: 10.1175/JPO-D-17-0048.1

Rühs, S., V. Zhurbas, I. Koszalka, J. Durgadoo, and A. Biastoch, 2017: Eddy diffusivity estimates from Lagrangian trajectories simulated with ocean models and surface drifter data - a case study for the greater Agulhas system. J. Phys. Oceanogr. doi:10.1175/JPO-D-17-0048.1, in press.

Eddy diffusivity estimates from Lagrangian trajectories simulated with ocean models and surface drifter data – a case study for the greater Agulhas system

Siren Rühs[1a], Victor Zhurbas[2], Inga M. Koszalka[13], Jonathan V. Durgadoo[1], Arne Biastoch[1]

[1] GEOMAR Helmholtz Centre for Ocean Research Kiel, Düsternbrooker Weg 20, Kiel, Germany

[2] Shirshov Institute of Oceanology, Nakhimovsky Prospect, 36, 117998 Moscow, Russia

[3] Christian-Albrechts University of Kiel, Germany

[a] sruehs@geomar.de

Abstract

The Lagrangian analysis of sets of particles advected with the flow fields of ocean models are used to study connectivity, i.e. exchange pathways, timescales and volume transports, between distinct oceanic regions. One important factor influencing the dispersion of fluid particles and hence connectivity is the Lagrangian eddy diffusivity, which quantifies the influence of turbulent processes on the rate of particle dispersal. Due to spatial and temporal discretization, turbulence is not fully resolved in modelled velocities, and the concept of eddy diffusivity is used to parametrize the impact of unresolved processes. However, the relations between observational- and model-based Lagrangian eddy diffusivity estimates as well as eddy parameterizations are not clear.

This study presents an analysis of the spatially variable near-surface lateral eddy diffusivity estimates obtained from Lagrangian trajectories simulated with 5-day mean velocities from an eddy-resolving ocean model (INALT01) for the Agulhas system. INALT01 features diffusive regimes for dynamically different regions, some of which exhibit strong suppression of eddy mixing by mean flow, and is consistent with the pattern and magnitude of drifter-based eddy diffusivity estimates. Using monthly-mean velocities decreases the estimated diffusivities less than eddy kinetic energy, supporting the idea that large and persistent eddy features dominate eddy diffusivities. For a non-eddying ocean model (ORCA05), Lagrangian eddy diffusivities are greatly reduced, in particular when the Gent and McWilliams parameterization of mesoscale eddies is employed.

1. Motivation

Over the last decades, the Lagrangian analysis of fluid motion by following floating instruments has been used to investigate ocean general circulation patterns (e.g. Davis 1991a,b; Poulain 2001; Lumpkin and Johnson 2013; Lumpkin et al. 2017). Additionally, an increasing amount of Lagrangian analyses is performed by advecting virtual fluid particles with the simulated flow fields of ocean models (van Sebille et al. submitted). They are employed in large-scale oceanography to study the sources, fate and transformation of water masses (Speich et al. 2001; Lique et al. 2010; Koszalka et al. 2013a,b; Gary et al. 2014; Durgadoo et al. 2017) and are particularly suited to quantify connectivity between different oceanic sites, i.e. preferential linking pathways (e.g. Rühs et al. 2013; van Sebille et al. 2013, 2014), associated timescales (e.g. Blanke et al. 2002; van Sebille et al. 2011; Koszalka et al. 2013a; Rühs et al. 2013), as well as volume, freshwater and heat transports (e.g. Blanke et al. 2001; Biastoch et al. 2008b; Döös et al. 2012).

One important factor influencing large-scale (~1000 km) connectivity is the average rate at which particles disperse. Turbulent processes, such as mesoscale (10-100 km) eddies and jets, cause fluid particles to disperse quickly and increase the rate of mass, momentum, and tracer spreading, leading to accelerated mixing (LaCasce 2008). Turbulent flow is often described via Reynolds decomposition in terms of a long-term (or slowly varying) "mean" velocity and the residual eddy component. Analogously, the concept of Lagrangian eddy diffusivity is used to quantify the rate of dispersal related to the cumulative effect of eddies. Depending on the definition of the "mean" flow, the residual eddy component may include not only mesoscale, but also seasonal to inter-annual (Rieck et al. 2015; Laurindo et al. 2017; Uchida et al. 2017) or smaller scale (if resolved but not lowpass-filtered) variability, or may specifically refer to processes not resolved by a certain flow field (Rypina et al. 2016). In this study we focus primarily on mesoscale eddy variability.

Owing to spatial and temporal discretization, turbulent processes are not fully resolved in modelled velocity fields, but parametrized instead. Simulated advective Lagrangian trajectories capture the resolved turbulence, but only implicitly include the effect of sub-grid scale parameterizations acting on the tracer and momentum equations, i.e. by altered large-scale circulation pattern and along-track changes of temperature and salinity. This led to the notion that dispersal of advective Lagrangian trajectories is not sufficiently diffusive compared to particle dispersal in the real ocean. To circumvent this issue, Lagrangian diffusion parameterizations were introduced (Griffa 1996; Berloff and McWilliams 2002; Monti and Leuzzi 2010; Döös et al. 2011). These add an additional stochastic component to the advective particle displacements (or velocities or accelerations) and have already been employed in regional ocean circulation studies (De Dominicis et al. 2012; Koszalka et al. 2013b; Rypina et al. 2016).

However, compared to the vast amount of large-scale Lagrangian applications with ocean models, there are few comprehensive validations of eddy diffusivities associated with the simulated particle dispersal. Numerous studies presented eddy diffusivity estimates derived from drifter data (e.g. Krauss and Böning 1987; Davis 1991a,b; Swenson and Niiler 1996; Poulain 2001; Lumpkin and Flament 2001; Bauer et al. 2002; Zhurbas and Oh 2004; Sallée et al. 2008; Koszalka et al. 2011; Zhurbas et al. 2014; Peng et al. 2015). Likewise, several studies addressed the diffusivity estimation using Lagrangian trajectories simulated with velocity fields from eddy-resolving ocean models (e.g. McClean et al. 2002; Koszalka and Lacasce 2010; Griesel et al. 2010, 2014; Chen et al. 2014; Wolfram et al. 2015). Yet, there are only a handful of publications aiming at a quantitative comparison of eddy diffusivity estimates from drifter data and simulated trajectories (De Dominicis et al. 2012; Rypina et al. 2012, 2016). Also, the relations between Lagrangian eddy diffusivity estimates and the optimal choice of diffusivities to be used in stochastic Lagrangian parameterizations and in the Eulerian diffusion parameterizations employed in OGCM tracer equations are not well

82 understood (van Sebille et al. submitted). Unresolved issues concern the difficulty to
83 unequivocally define the "mean" flow and residual eddy component (Griesel et al. 2014), the
84 spatial variability of eddy diffusivities associated with different turbulence regimes (Berloff
85 and McWilliams 2002; Koszalka et al. 2011), and the sensitivity of model-based eddy
86 diffusivity estimates to the temporal and spatial model resolution (Keating et al. 2011;
87 Wolfram et al. 2015; van Sebille et al. submitted).

88 In this study, we address this gap by jointly assessing lateral near-surface eddy diffusivity
89 estimates obtained from real drifter data and trajectories simulated with the velocity output
90 from ocean general circulation models (OGCMs) at varying horizontal and temporal
91 resolution for the greater Agulhas system. The greater Agulhas system, located around the
92 southern tip of Africa, is known for its vigorous eddy activity and importance for interbasin
93 exchange of heat, salt, and momentum between the Indian and Atlantic Oceans (e.g. Beal et
94 al. 2011). It features different dynamic regimes in a confined region (Figure 1): the Agulhas
95 Current, a strong but stable western boundary current in the Indian Ocean, its retroflection
96 into the eastward flowing Agulhas Return Current, and associated shedding of Agulhas eddies
97 into the Atlantic (Lutjeharms 2006). Hence, it constitutes a good test region for evaluating
98 spatially variable eddy diffusivity characteristics. In particular, we address the following
99 questions:

100 (1) What are the characteristics of lateral near-surface eddy diffusivities estimated
101 from 2D-trajectories simulated with an eddy-resolving OGCM?
102 (2) How do these diffusivity estimates compare to those derived from drifter data?
103 (3) How sensitive are the diffusivity estimates to the temporal and horizontal
104 resolution of the underlying Eulerian OGCM velocity fields? And what is the
105 impact of the Gent and Mc Williams (GM) parametrization for baroclinic eddies in
106 a non-eddying OGCM on the diffusivity estimates?

This manuscript is structured as follows: In section 2, we describe the employed OGCMs, the offline performed Lagrangian experiments, the applied method for eddy diffusivity estimation, and the primary observational reference data set. In section 3, we present and discuss the results: eddy diffusivity estimates obtained from trajectories simulated with 5-day mean velocity output of an eddy-resolving OGCM (section 3.1), a comparison of those simulation-based estimates to the observation-based estimates (section 3.2), and the sensitivity of the simulation-based diffusivity estimates to the temporal and lateral OGCM output resolution, including the impact of an applied GM parametrization (section 3.3). In section 4, we further compare our diffusivity estimates with eddy diffusivity estimates based on different methods and discuss possible implications of our results for eddy parameterization approaches. Section 5 lists our conclusions.

2. Data and Methods

One major goal of this study is to compare eddy diffusivity estimates obtained from trajectories simulated with ocean models to those obtained from observed surface drifter data. Therefore, we calculated 2D Lagrangian trajectories resembling surface drifter tracks from the simulated flow fields of an eddy-resolving and a non-eddying global OGCM configuration, INALT01 and ORCA05, respectively. Subsequently, we derived eddy diffusivities from those simulated trajectories as well as from the Global Drifter Program (GDP; Lumpkin and Pazos, 2007) data following the method employed by Zhurbas et al. (2014). Zhurbas et al. (2014) already presented global maps of drifter-derived eddy diffusivities and our updated version of their estimates for the Agulhas region serves as the primary observational reference in this study.

2.1 Global Drifter Program data

The GDP array of satellite-tracked surface drifting buoys is the highest spatial resolution ocean velocity data currently available and it is the cornerstone of our knowledge of near-

surface submesoscale and mesoscale turbulence and turbulent diffusive regimes (Lumpkin et al. 2017). Each drifter consists of a surface buoy, with a transmitter and a temperature sensor, and a subsurface drogue centered at 15 m depth measuring near-surface mixed-layer currents. For this study we used the latitude, longitude and drifter velocity components at 6-h intervals obtained by objective interpolation (Hansen and Poulain 1996) updated through 2012 (data available at http://www.aoml.noaa.gov/phod/dac/gdp.html). Only trajectory segments with the drogue attached were considered (Lumpkin et al. 2013) and the trajectory data was low-pass filtered prior to the diffusivity calculations to remove variability in drifter positions and velocities with periods smaller than two days mostly caused by inertial oscillations.

2.2 Lagrangian trajectories from ocean model simulations

Ocean model simulations

The global ocean/sea-ice model configurations INALT01 and ORCA05 were developed under the DRAKKAR framework (The DRAKKAR Group 2007; Barnier et al. 2014). They were formulated with the Nucleus for European Modeling of the Ocean (NEMO, version 3.1.1; Madec 2008) and implemented on a horizontal tripolar Arakawa C-grid (Mesinger and Arakawa 1976), which is Mercator-type south of 20°N. Both employed configurations have 46 vertical levels with grid spacing increasing from 6 m at the surface to 250 m at depth and partially filled bottom cells.

ORCA05 is a well-validated global configuration (e.g. Danabasoglu et al. 2014) with a nominal horizontal resolution of 0.5° (~43 km in the Agulhas region), which realistically represents the mean flow and interannual to decadal variability of the large-scale circulation (Biastoch et al. 2008a). It is a non-eddying OGCM configuration as to fully capture the mesoscale variability in the Agulhas region horizontal resolutions of 0.25° and finer are needed (Hallberg 2013).

INALT01 is a two-way nested model configuration, which is based on the global ORCA05 configuration described above, but regionally refined between 50°S – 8°N and

159 70°W – 70°E to its nominal horizontal resolution of 0.1° (~9 km in Agulhas region) to
160 capture the complex mesoscale dynamics of the greater Agulhas system (Durgadoo et al.
161 2013). Figure 1a shows a snapshot of the daily mean current speed at 15m depth, illustrating
162 the ability of the model to represent e.g. Mozambique Channel eddies and Agulhas rings.
163 INALT01 has been employed by a variety of studies investigating the local dynamics (Cronin
164 et al. 2013; Loveday et al. 2014) and large-scale impact (Lübbecke et al. 2015; Biastoch et al.
165 2015) of the greater Agulhas system.

166 Both ocean/sea-ice models were spun-up for twenty years before the actual simulations
167 were performed using interannually varying (years 1948-2007) or climatological atmospheric
168 forcing fields from the Common Ocean–Ice Reference Experiments, version 2b (CORE v2b,
169 Large and Yeager 2008; Griffies et al. 2009). The evolution of tracers was simulated using a
170 Laplacian iso-neutral diffusion operator and the total variance dissipation (TVD, Zalesak
171 1979) advection scheme. The momentum equations were formulated using a bi-Laplacian
172 lateral diffusion operator and the energy and enstrophy conserving (EEN, Arakawa and Hsu
173 1990) advection scheme. Diffusivity and viscosity coefficients vary horizontally according to
174 the local grid size and are specified via their maximum values A_{ht0} and A_{hm0} (Table 1). Further
175 details of the INALT01 and ORCA05 simulations employed in this study are described in
176 Durgadoo et al. (2013).

177 Table 1 contains a summary of the model simulations providing velocity data used for 6
178 Lagrangian experiments performed for this study. Note that: 1) one simulation with the
179 eddying INALT01 configuration yielded three different Lagrangian experiments that differ
180 only in the temporal resolution of the velocity fields used for the trajectory integration
181 (SIMeddy-1d, SIMeddy-5d, SIMeddy-1m); and 2) for the non-eddying ORCA05
182 configurations two simulations and respective Lagrangian experiments were analyzed, one
183 with (SIMpareddy-5d) and one without (SIMnoeddy-5d) Gent and Mc Williams (GM, 1990)
184 parametrization of baroclinic eddies. The GM parameterization mimics the impact of

baroclinic eddies on tracer fluxes by adding an extra term to the tracer equation which represents eddy induced advection (Gent et al. 1995; Gent 2011); it is determined by the GM coefficient, which is computed from the growth of the baroclinic instability as described in Treguier et al. (1997), and is allowed to vary horizontally and temporally with a cap of 1000 $m^2 s^{-1}$.

Lagrangian trajectory integration

The trajectory integration was performed using the offline Lagrangian community tool ARIANE (version 2.2.6, Blanke and Raynaud, 1997). Lagrangian particles were released homogenously over the greater Agulhas system (Figure 1) at ~15 m depth, every 0.5° in both, latitudinal and longitudinal directions, every 30 days for ten years (beginning at January the 15th 1996, 12:00), yielding nearly 900,000 particles for each Lagrangian experiment. Subsequently particles were advected forward in time for 60 days with the modelled horizontal velocities (for SIMpareddy-5d the Eulerian velocity combined with the eddy-induced velocity from the GM parameterization was used), whereby particle positions were stored daily. As drogued surface drifters' behavior should be mimicked, particles were kept at the same depth over the whole integration period. No additional stochastic Lagrangian parameterization was employed.

The resulting trajectories represent pathways determined by the resolved Eulerian flow, or, in case of SIMpareddy-5d, by the resolved Eulerian flow combined with the mesoscale eddy induced velocity from the GM parameterization. It has been shown that including the mesoscale eddy induced transport yields a more realistic picture of the mean overturning circulation, in particular in the Southern Ocean, where the eddy-induced meridional velocity counteracts the Eulerian meridional velocity (e.g. Drijfhout et al. 2003). However, while parameterizing the advective effect of baroclinic eddies where they are not resolved by the model, GM also suppresses the explicit generation of physical as well as numerical mesoscale variability (Hallberg 2013) by flattening isopycnals. Thus, it is worth

comparing eddy diffusivity estimates from Lagrangian experiments in non-eddying ocean model simulations with- and without GM parametrization.

2.3 Lagrangian eddy diffusivity estimation

Lagrangian eddy diffusivities can be estimated from both single-particle and particle-pair/cluster statistics (LaCasce 2008a). While particle-pair/cluster statistics are additionally suited to infer the spatial spectra of mesoscale currents, they also require a simultaneous deployment of a large number of particles in a confined area. Since, at present, GDP data fulfills this requirement only in a few regions and thus cannot be used to infer spatial variability of eddy diffusivity estimates via particle-pair or cluster statistics, we employed single-particle statistics.

Theoretical background of single-particle diffusivity estimation

The concept of Lagrangian diffusivity estimation has been introduced by Taylor (1922), who determined scalar single-particle diffusivities by integrating the ensemble-mean Lagrangian velocity autocorrelation function:

$$k^{Taylor} = \lim_{t\to\infty} k(t) \tag{1}$$

$$k(t) = 0.5\frac{d}{dt}\langle \mathbf{d}(t)^2\rangle_L = \langle \mathbf{v_L}(t)\cdot\mathbf{d}(t)\rangle_L = \int_{t_0}^{t}\langle \mathbf{v_L}(t)\cdot\mathbf{v_L}(\tau)\rangle_L\, d\tau \tag{2}$$

Whereby $\mathbf{d}(t) = \mathbf{x}(t) - \mathbf{x}(t_0) = \int_{t_0}^{t}\mathbf{v_L}(\tau)d\tau$ represents the particle displacement, $\mathbf{v_L}(t) = \partial\mathbf{x}/\partial t$ is the Lagrangian velocity, and $\langle\ \ \rangle_L$ indicates Lagrangian averaging, i.e. averaging over an ensemble of particles at a certain time lag *t* after their release at t_0.

The Taylor approach was formulated in the idealized context of statistically homogeneous, stationary and isotropic flows. Davis (1991b) extended the Taylor framework for single-particle diffusivity estimation over inhomogeneous and anisotropic flows by introducing the eddy diffusivity tensor. The diffusivity is then calculated for an ensemble of particles originating at a certain location, or within a specified geographical region where the flow can be assumed as locally homogenous, for each tensor component $k_{jk}(\mathbf{x}, t)$ individually

(j, k are the indices for the horizontal dimensions in Cartesian space with j, k $\in (1,2)$). Instead of the absolute, only the residual velocities $\mathbf{v_L}'(t|\mathbf{x}, t_o)$ and displacements $\mathbf{d}'(t|\mathbf{x}, t_o)$ for each particle (passing through $\mathbf{x}$ at time t_0) are considered. The residual velocity is defined as the departure from the local Eulerian mean velocity; the residual displacement is defined as the total displacements minus that due to the Eulerian mean velocity. This is why, strictly speaking, the eddy diffusivity is not a pure Lagrangian, but a mixed Eulerian-Lagrangian statistic (LaCasce 2008a).

Single-particle eddy diffusivity estimation thus involves the following steps: a) binning of particle trajectories on a longitudinal-latitudinal grid; b) estimation of the "mean" flow and subsequent calculation of residual Lagrangian velocities and/or displacements; c) estimation of the ensemble-mean eddy diffusivity tensor components for each bin (either in fixed coordinate or along- and across-flow directions).

There are various approaches to estimate the components of the single-particle eddy diffusivity tensor $k_{jk}(\mathbf{x}, t)$, all deriving from Taylors' and Davis diffusivity concepts, but using different procedures to reduce potential biases caused by the inhomogeneity and nonstationarity of flows, i.e. different binning techniques, "mean" flow definitions, and diffusivity estimators. Lagrangian averaging is performed using geographical bins (e.g. Swenson and Niiler 1996; Sallée et al. 2008), which may additionally overlap and/or be rotated with respect to the velocity variance axis (e.g. Lumpkin and Garzoli 2005; Peng et al. 2015); Alternatively, trajectories may be clustered according to the nearest-neighbor distance (Koszalka and Lacasce 2010). The mean flow is estimated either by simple averaging or includes advanced techniques such as spline-fitting or Gauss-Markov decomposition (e.g. Bauer et al. 2002; Laurindo et al. 2017). Finally, diffusivity is estimated via the half-growth rate of the residual dispersion tensor (e.g. de Verdiere 1983; Oh et al. 2000; Rypina et al. 2012, 2016), the integral of the residual velocity autocorrelation (e.g. Koszalka et al. 2011;

Peng et al. 2015), or the residual velocity-displacement tensor (e.g. Davis 1991b; Swenson and Niiler 1996; Oh et al. 2000).

Single-particle eddy diffusivity estimation following Zhurbas et al. (2014)

In this study, we follow the approach for diffusivity estimation used by Zhurbas et al. (2014). This approach was first introduced and thoroughly tested by random-flight simulations of Lagrangian trajectories in a sheared flow (Oh et al. 2000) and later employed in an improved version accounting for the mean flow suppression of eddy diffusivities by Zhurbas et al. (2014). Assuming isotropy in diffusivities/eddy statistics, the approach yields one time-lag and coordinate dependent *scalar lateral eddy diffusivity* $K(\mathbf{x}, t)$, which is defined as the semi-sum of the minor principal component of the symmetric part of the Davis diffusivity tensor ($k_{p2}^{davis}(\mathbf{x}, t)$) and the half growth rate of the minor principal component of the single-particle dispersion tensor ($k_{p2}^{disp}(\mathbf{x}, t)$), thus combining two frequently used approaches for diffusivity estimation:

$$K(\mathbf{x}, t) = (k_{p2}^{davis}(\mathbf{x}, t) + k_{p2}^{disp}(\mathbf{x}, t))/2 \tag{3}$$

The *Davis diffusivity tensor* $k_{jk}(\mathbf{x}, t)$ is defined as

$$k_{jk}(\mathbf{x}, t) = -\langle {v_{Lj}}'(t_0|\mathbf{x}, t_o) \cdot {d_k}'(t_0 - t|\mathbf{x}, t_o)\rangle_L \tag{4}$$

whereby the notation ${d_i}'(t_0 - t|\mathbf{x}, t_o)$ represents the residual displacement for a particle passing through $\boldsymbol{x}$ at time t_0, obtained from following its trajectory backward in time for the period $[t_0 - t, t_0]$. To avoid rotational eddy fluxes, which are non-diffusive, only the symmetric part of $k_{jk}(\mathbf{x}, t)$ is considered, which is here referred to as $k_{jk}^{davis}(\mathbf{x}, t)$:

$$k_{jk}^{davis}(\mathbf{x}, t) = (k_{jk}(\mathbf{x}, t) + k_{kj}(\mathbf{x}, t))/2 \tag{5}$$

The *half growth rate of the single-particle dispersion tensor* $s_{jk}(\mathbf{x}, t)$ is defined as

$$k_{jk}^{disp}(\mathbf{x}, t) = 0.5\frac{\delta s_{jk}}{\delta t} \tag{6}$$

$$s_{jk}(\mathbf{x}, t) = \langle {d_j}'(t_0 + t|\mathbf{x}, t_o) \cdot {d_k}'(t_0 + t|\mathbf{x}, t_o)\rangle_L \tag{7}$$

whereby the notation $d_i'(t_0 + t|\mathbf{x}, t_o)$ represents the residual displacement of a particle passing through $\boldsymbol{x}$ at time t_0 obtained from following its trajectory forward in time for the period $[t_0, t_0 + t]$. The dispersion tensor is symmetric by construction and does not include rotational and advective eddy fluxes.

If diffusivities are estimated from ensembles of trajectories passing through a fixed position **x** at different times, $k_{jk}^{davis}(\mathbf{x}, t)$ yields the true time-lag dependent diffusivity, whereas $k_{jk}^{disp}(\mathbf{x}, t)$ can be biased by the shear effect. However, the limited spatial-temporal resolution of surface drifter data only allows for estimating diffusivities from ensembles of particles passing through a finite vicinity of **x,** in which case both measures can be positively biased by shear. Since Oh et al. (2000) showed that the minor principal components of $k_{jk}^{disp}(\mathbf{x}, t)$ and $k_{jk}^{davis}(\mathbf{x}, t)$, representing across-flow diffusivities (cf. Peng et al. 2015), are less biased by shear flow, these were chosen as (the only) representative estimates for lateral eddy diffusivities. They were obtained according to

$$k_{p2}(\mathbf{x}, t) = k_{xx}(\mathbf{x}, t)sin^2\theta - k_{xy}(\mathbf{x}, t)sin2\theta + k_{yy}(\mathbf{x}, t)cos^2\theta \quad (8)$$

$$tan2\theta = 2k_{xy}(\mathbf{x}, t)/(k_{xx}(\mathbf{x}, t) - k_{yy}(\mathbf{x}, t) \quad (9)$$

Consistently with Zhurbas et al. (2014) we used this approach to estimate lateral eddy diffusivities from all Lagrangian experiments and surface drifter data in overlapping 5° x 5° bins with a 2° offset in longitudinal and latitudinal direction. Residual velocities were calculated relative to climatological monthly mean currents. That means, for each bin for each month of the year, all trajectories passing that bin in the respective month were selected. Then, all trajectory positions within the bin were considered as the origin of a pseudo-trajectory (overlapping pseudo-tracks were removed) and individual backward and forward displacements $\mathbf{d}(t|\mathbf{x}, t_o)$ as well as the Lagrangian velocity at the pseudo-origin $\mathbf{v_L}(t_0|\mathbf{x}, t_o)$ were calculated (for the simulated trajectories Lagrangian velocities were obtained by central time-differencing of the discrete displacements). Ensemble averaging

yielded the mean displacement $\langle \mathbf{d}(t) \rangle_L$ and the climatological monthly mean velocity $\langle \mathbf{v_L}(t_0) \rangle_L$ that were used to derive the residual velocities and displacements as

$$\mathbf{v_L}'(t_0|\boldsymbol{x}, t_o) = \mathbf{v_L}(t_0|\mathbf{x}, t_o) - \langle \mathbf{v_L}(t_0) \rangle_L \quad (10)$$

$$\mathbf{d}'(t|\boldsymbol{x}, t_o) = \mathbf{d}(t|\boldsymbol{x}, t_o) - \langle \mathbf{d}(t) \rangle_L \quad (11)$$

From these, for each set of pseudo-trajectories starting in the same month $k_{jk}^{davis}(\mathbf{x}, t)$, $k_{jk}^{disp}(\mathbf{x}, t)$, and $K(\mathbf{x}, t)$ were estimated; the final diffusivity estimates were obtained as averages of the respective twelve individual estimates. Further details of the calculation, including smoothing details and small modifications with respect to the original Zhurbas et al. (2014) approach, are discussed in Appendix 1.

It is important to note the time-lag dependence of diffusivity estimates. Again, following Zhurbas et al. (2014), we distinguish the maximum diffusivity $K_{max,}$ defined as the local maximum of $K(\mathbf{x}, t)$ within the time lag interval 1day ≤ t ≤ 20days, and the asymptotic diffusivity $K_{inf,}$ defined as the local mean value of $K(\mathbf{x}, t)$ for the time lag interval 15days ≤ t ≤ 20days (Figure 2). The usage of larger time lags was avoided since the sampling error and potential biases caused by spatial and/or temporal inhomogeneity of the residual velocity field increase with time lag (Davis 1991b).

From a physical or parametrization point of view, K_{inf} is the sought-after estimate of diffusivity, since at those large time lags the mean residual distance travelled by a fluid parcel in a certain time interval is approximately proportional to the square-root of that time interval, just as for a diffusive process in which fluid parcels undergo random walks (cf. discussion of the Lagrangian integral timescale below). Earlier studies used K_{max} (e.g. Oh et al. 2000; Lumpkin and Flament 2001; Sallée et al. 2008), but recently it has been shown that K_{max} can largely overestimate the "true" diffusivity due to a suppression of mixing in areas where eddies and mean flow propagate at different speeds (Griesel et al. 2010; Klocker et al. 2012a,b; Wolfram et al. 2017).

In this work, we purposefully assess both K_{inf} and K_{max} since the relation of the two quantifies the strength of diffusivity suppression by mean flow (Klocker et al. 2012a), and thus can be used to diagnose how well the ocean models represent these effects (i.e. the relationship between the mean flow and the eddy propagation speed along the mean flow).

2.4 Pseudo-Eulerian EKE, Lagrangian eddy time and length scales

In addition to Lagrangian eddy diffusivities, the pseudo-Eulerian mean EKE and Lagrangian eddy integral time (T_L) and length (L_L) scales were calculated in overlapping 5° x 5° bins.

To be consistent with the definition of the eddy diffusivity, for which we only considered the minor principal component (i.e. the across-flow component), the *pseudo-Eulerian mean EKE* is defined as the minor principal component of the Lagrangian mean residual velocity covariance matrix at zero time lag $\langle v_{Lj}'(t_0|\mathbf{x},t_o)\cdot v_{Lk}'(t_0|\mathbf{x},t_o)\rangle_L$.

Mixing and thus K_{inf} can generally be represented as scaling with EKE and the time scale T_L over which mixing occurs, or equivalently, as scaling with the distance L_L a particle would travel with the characteristic root mean square eddy velocity v' (which equals $\sqrt{EKE}$) before it mixes with its surroundings: $K = EKE\ T_L = \sqrt{EKE}\ L_L$ (cf. LaCasce 2008b). Analogously, we estimated T_L and L_L using our asymptotic diffusivity estimate K_{inf} and pseudo-Eulerian mean EKE as

$$T_L = K_{inf}/EKE \tag{12}$$

$$L_L = K_{inf}/\sqrt{EKE} \tag{13}$$

T_L and L_L represent "memory" scales over which Lagrangian residual velocities stay strongly correlated; at time and space scales much larger than T_L and L_L, respectively, residual single-particle dispersion resembles diffusive spreading.

3. Results and Discussion

3.1 Eddy diffusivity estimates derived from trajectories simulated with an eddying ocean model

In this section we present and discuss near-surface lateral eddy diffusivity estimates obtained from residual velocities and displacements of Lagrangian trajectories simulated with the 5-day mean velocity output of the eddy resolving INALT01 hindcast experiment (Lagrangian experiment SIMeddy-5d).

Time lag dependence of eddy diffusivity estimates

Figure 2 shows time lag dependent ensemble mean single-particle residual dispersion and eddy diffusivity estimates for four selected 5° x 5° bins representing different dynamic regimes (Figure 1). Table 2 lists the respective pseudo-Eulerian and Lagrangian statistics. The bins are located in the eastern South Atlantic Gyre (eSAG), Agulhas Return Current (ARC), Agulhas Retroflection (AR), and Agulhas Current (AC).

The eSAG is an open ocean region characterized by weak mean flow and low EKE. Its dispersion and diffusivity curves (Figure 2a,e) show the characteristic asymptotic behavior described in classical turbulence theory (LaCasce 2008): At time lags larger than ~20 days $s_{p2}(t)$ grows approximately linear with time (meaning the mean residual displacement of a fluid parcel in a certain time interval is approximately proportional to the square root of that time interval), typical for the diffusive regime. Consequently, across-flow eddy diffusivities asymptotically approach a nearly constant value at those time lags and $K_{max} \approx K_{inf} \approx 1.5 \times 10^3$ $m^2 s^{-1}$. Since the curves for $s_{yy}(t)$ and $s_{p2}(t)$ are hardly distinguishable, and even $s_{xx}(t)$ shows a similar behavior, we conclude that the spreading is approximately isotropic. In this particular case, with weak influence of mean flow and nearly isotropic particle spreading, the diffusivity estimates $k_{p2}^{disp}(t)$, $k_{p2}^{davis}(t)$, and $K(t)$ yield nearly the same results, with only a small spread towards larger time lags.

The ARC is a strong along-front current with pronounced meridional excursions, supposedly related to changes in bottom topography, and vigorous mesoscale variability (Lutjeharms and Ansorge 2001). In the ARC region dispersion and diffusivity curves (Figure 2b,f) differ substantially from those described for the eSAG. They can be considered typical of a region where eddies propagate westward relative to an eastward mean flow (Boebel et al. 2003; Chelton et al. 2011). On one hand, the instability of the ARC introduces high EKE, leading to an overall increased across-flow eddy diffusivity. On the other hand, the across-flow eddy diffusivity is suppressed by the mean flow, as shown conceptually for the ACC by Klocker et al. (2012a). $s_{p2}(t)$, which is nearly identical to $s_{yy}(t)$, increases fast at short time lags, but then levels off before finally increasing again approximately linearly with time. This yields across-flow eddy diffusivity curves to peak (and slightly oscillate) at short time lags before reaching their asymptotic value; the maximum diffusivity strongly overestimates the asymptotic diffusivity, $K_{max} \approx 12.2 \times 10^3$ and $K_{inf} \approx 3.0 \times 10^3$ m^2 s^{-1}. Still, the diffusivity estimates $k_{p2}^{disp}(t)$ and $k_{p2}^{davis}(t)$ yield nearly the same results, introducing only a small spread around $K(t)$ towards larger time lags.

The dispersion and diffusivity curves for the AR (Figure 2c,g) show a very similar behavior to that described for the ARC, but with even higher diffusivity values, related to a regional maximum in EKE (cf. Figure 1d). The across-flow eddy diffusivity curves peak at short time lags before reaching their asymptotic values. Thus, as for the ARC, the maximum diffusivity overestimates the asymptotic diffusivity, $K_{max} \approx 21.8 \times 10^3$ and $K_{inf} \approx 11.2 \times 10^3$ m^2 s^{-1}. However, the result for K_{inf} should be interpreted with caution, since, even though $k_{p2}^{disp}(t)$ and $k_{p2}^{davis}(t)$ show a similar temporal evolution, their spread around the combined estimate $K(t)$ increases after their reached their maximum value. Their respective asymptotic diffusivity estimates K_{inf}^{disp} and K_{inf}^{davis} are 8.1×10^3 and 14.4×10^3 m^2 s^{-1}, respectively.

The AC, heading southwestward, is one of the strongest western boundary currents of the world ocean. However, in contrast to other western boundary currents, such as the Kuroshio or the Gulf Stream, it is remarkably stable (Lutjeharms 2006, 2007) and has lower EKE. The dispersion and diffusivity curves obtained for the AC (Figure 2d,h) most resemble those of the eSAG, without strong suppression of eddy mixing by mean flow. This indicates that local eddies propagate at approximately the same speed and in the same direction of the mean flow, which is indeed the case for Natal pulses and Mozambique eddies travelling within and at the border of the AC (Schouten et al. 2002). In contrast to open-ocean currents like the AR/ARC, where eddies can propagate westward separately from the mean flow, westward drift is impossible in the AC due to topographic constraints. However, at larger time lags, $s_{p2}(t)$ does not increase linearly. Consequently, $k_{p2}^{disp}(t)$ does not show an asymptotic behavior but steadily increases with increasing time lag, suggesting that the mean flow was not successfully removed. Moreover, $k_{p2}^{davis}(t)$ shows a different behavior: it reaches its maximum at a time lag of ~5 days and afterwards slowly decreases with increasing time lag. Neither the asymptotic nor the maximum diffusivity can be determined unambiguously.

In general, the results for the eSAG and ARC (and with some limitations also those for the AR) suggest, that even in a complex eddying flow system as represented by the greater Agulhas system with strong eddy-mean flow interaction, asymptotic diffusive regimes can be found. However, the results for the AC also highlight the limitations of a generalized binning method to quantify lateral eddy dispersion and diffusivity. Due to the spatial and probably also the temporal inhomogeneity of the residual velocity field, the eddy dispersion does not reach a diffusive regime everywhere, and the derived eddy diffusivity estimates are sensitive to the applied method.

We note that the time lag interval chosen for the calculation of asymptotic diffusivity estimates adopted from Zhurbas et al. (2014) for their global analysis of surface drifters is not

perfectly suited for the simulated trajectories in the greater Agulhas system, since the diffusivities do not yet convergence in all cases. In particular, for the eSAG bin the Lagrangian integral time scale is ~11.6 days (Table 2), indicating that the diffusive regime is only reached at substantially larger time lags (section 2.4; LaCasce 2008). Indeed, convergence seems to be reached at time lags between 25 and 30 days. Yet, as changing the averaging interval does not impact the estimates substantially, we keep them as in Zhurbas (2014) for the sake of comparison.

Spatial pattern of eddy diffusivity estimates

Figures 3a,d,g show the spatial pattern of asymptotic eddy diffusivity estimates for the whole greater Agulhas system. The individual estimates K_{inf}^{davis} and K_{inf}^{disp} show the same general pattern and magnitude as the combined estimate K_{inf}: Highest eddy diffusivities are found around the AR region (cf. Figure 2g), an area with strong unstable mean flow and high EKE (Figure 1c and 5c). Relatively high eddy diffusivities also occur in regions with weaker background flow, but still high EKE, such as in the Cape Basin around the major pathway for Agulhas Rings (Schouten et al. 2000; Dencausse et al. 2010), and in the region west and south of Madagascar, where Mozambique Channel Eddies and South East Madagascar Eddies propagate (Schouten et al. 2002). In the strong but relative stable Agulhas Current, eddy diffusivities are lower due to high mean kinetic energy but comparatively low EKE. In the vicinity of the ARC (cf. Figure 2f), diffusivities are further decreased, despite locally high EKE (Figure 1c and 5c). Lowest diffusivities occur around the low-energy eSAG region.

The spatial pattern of the maximum diffusivity estimates, as exemplarily shown for the combined estimate K_{max} in Figure 4a, is similar to that of the asymptotic diffusivity estimates. However, despite a general increase in magnitude, the spatial pattern of K_{max} better resembles that of EKE. In particular, the region around the ARC shows strongly elevated diffusivities. The pronounced differences between K_{max} and K_{inf} in this region can be interpreted as the imprint of eddy mixing suppression by mean flow as already discussed exemplarily for the

ARC bin (section 2.1). The relation K_{max}/K_{inf} displayed in Figure 4d highlights all areas where K_{max} greatly overestimates K_{inf} and thus where eddy mixing suppression is strong. The region around the ARC clearly stands out, but also in the northern part of the Antarctic Circumpolar Current (ACC) eddy mixing suppression is apparent. This fits well to the theory of eddy mixing, since both regions feature an eastward mean flow and the possibility for westward propagation of eddies.

Averaging over all spatial bins yields diffusivities of ~3.3 x 10^3, ~3.5 x 10^3, and ~3.4 x 10^3 m^2 s^{-1} for K_{inf}^{davis}, K_{inf}^{disp}, and K_{inf}, respectively. Even though the spatially averaged K_{inf}^{disp} constitutes a slightly higher estimate than the spatially averaged K_{inf}^{davis}, local differences between K_{inf}^{davis} and K_{inf}^{disp} vary in sign and magnitude. Largest discrepancies are found in the AR and ARC regions, where diffusivities differ by up to more than 5.0 x 10^3 m^2 s^{-1} (Table 3). Furthermore, local discrepancies in K_{inf} are higher than those in K_{max} (not shown), highlighting the difficulty to capture convergence of the diffusivity estimates. Even though the approach introduced by Oh et al. (2000) and formulated in its refined form by Zhurbas et al. (2014) seems to be applicable in most regions, the combined diffusivity estimate $K(\mathbf{x}, t)$ should be interpreted with caution for areas with big discrepancies between the two individual diffusivity estimates.

3.2 Comparison of eddy diffusivity estimates derived from simulated trajectories and drifter data

In this section we compare diffusivity estimates obtained from Lagrangian experiment SIMeddy-5d with those obtained from drifter data (OBS). A comparison with other observational-based eddy diffusivity estimates calculated with alternative techniques is given in section 4.

Estimates of K_{inf} and K_{max} obtained from OBS and SIMeddy-5d show a good agreement in their spatial pattern (Figures 3,4); averaging over all spatial bins yields values for K_{inf} (K_{max})

472 of ~3.4 x 10^3 (~5.2 x 10^3) and ~4.1 x 10^3 (~6.0 x 10^3) m^2 s^{-1}, for SIMeddy-5d and OBS,
473 respectively.

474 For nearly the whole greater Agulhas system pseudo-Eulerian mean EKE (Figure 5c,d,f,
475 Table 2,3) is lower in SIMeddy-5d than in OBS, indicating that the on average slightly lower
476 diffusivity values in SIMeddy-5d are mainly related to a weaker mesoscale variability.
477 Averaging over all spatial bins yields 197 and 307 cm^2 s^{-2} for SIMeddy-5d and OBS,
478 respectively. Possible reasons for this discrepancy are the following: First, there are known
479 weaknesses of the model configuration. The EKE in the open ocean is too low in most model
480 simulations due to un- or under-resolved processes, and it is further decreased in ocean model
481 simulations forced with relative winds, such as those employed in this study, due to enhanced
482 surface drag (Eden and Dietze 2009). A limited representation of the depth-dependent Ekman
483 drift in view of a too scarce vertical grid spacing (6 m at the surface) of the model may have
484 further contributed to lowered EKE values (this follows from the fact that the kinetic energy
485 of a layer with velocity shear always exceeds the kinetic energy of a layer of the same
486 thickness and momentum, but with uniform velocity). Second, the discrepancy between OBS
487 and SIM could be partially related to the nature of surface drifters, which, despite being
488 drogued at 15m depth, do not perfectly follow the local current, but experience some
489 additional wind-induced drift (Lumpkin and Pazos 2007; Poulain et al. 2009). Finally, the
490 different spatio-temporal coverage of drifter data and simulated trajectories matters
491 (Supplementary). However, keeping in mind that one-to-one comparisons of drifters and
492 simulated trajectories are of limited use for non-assimilative models (cf. van Sebille et al.
493 2009), a much better agreement between SIMeddy-5d and OBS seems unlikely, even if the
494 sampling of simulated trajectories would be adjusted to fit the one of drifter data. Also, the
495 choice of the overall time period seems to be of minor importance, since diffusivity estimates
496 obtained from Lagrangian experiment SIMeddy5d hardly differ from Lagrangian experiment
497 SIMeddy-5d-clim (Figures 6a,7, Table 3), which is identical to SIMeddy-5d despite for the

fact that the OGCM was forced with climatological atmospheric fields instead of interannually varying ones. This indicates an only minor impact of interannual to decadal variability on the diffusivity estimates - at least in the region of interest.

Despite lower mean diffusivities in SIMeddy-5d compared to OBS, we cannot conclude that trajectories simulated with SIMeddy-5d are generally not sufficiently diffusive, because locally, the difference between SIMeddy-5d and OBS strongly varies in magnitude and sign.

Since the general pattern of the difference between SIMeddy-5d and OBS is robust with respect to the method employed for diffusivity estimation (Figure 3c,f,i), a closer investigation of this pattern is justified. One can distinguish regions where 1) K_{max} and K_{inf} are lower in SIMeddy-5d than in OBS, such as in the eSAG (Table 2) or South of Madagascar; 2) K_{max} and K_{inf} are higher in SIMeddy-5d than in OBS, such as in a broad region west of the retroflection; 3) K_{max} is lower, but K_{inf} is higher in SIMeddy-5d than in OBS, such as northwest of the retroflection; and 4) K_{inf} is lower, but K_{max} is higher in SIMeddy-5d than in OBS, such as in parts of the ARC (Table 2) and at the southern boundary of the study region. In the third and fourth case, the local relation K_{max}/K_{inf} is substantially altered (Figure 4d,e,f), implying that the local representation of eddy mixing suppression differs (e.g., in the region around the ARC, eddy mixing suppression is higher in SIMeddy-5d than in OBS). This is most likely related to the fact that the local pseudo-Eulerian mean flow sampled by SIMeddy-5d clearly features a coherent eastward current, whereas in OBS, the mean flow pattern is less clear (Figure 5a,b).

We conclude that differences in the near-surface lateral eddy diffusivity estimates between SIMeddy-5d and OBS cannot be directly linked to differences in EKE, but are also influenced by differences in Lagrangian eddy length and time scales related to the suppression of eddy mixing. Even though local differences between the diffusivity estimates from SIMeddy-5d and OBS are strongly non-uniform and can be relatively high, the frequency distributions of K_{inf} are remarkably similar (Figure 7, Table 3). Moreover, differences

between SIMeddy-5d and OBS seem to fall in the uncertainty range. Differences between the two methods to estimate lateral diffusivities in SIMeddy-5d are of the same magnitude as differences between SIM and OBS (cf. section 3.1, Table 2); differences between various observational approaches estimating near-surface lateral eddy diffusivity, e.g., in the ACC region, are of comparable magnitude or even bigger (Klocker et al., 2012b and references therein). Thus, we conclude that the Lagrangian trajectories simulated with the 5-day mean output of the high-resolution ocean model INALT01 (SIMeddy-5d) capture Lagrangian eddy diffusivity characteristics of real drifter data fairly well, without the need for additional random-walk diffusion.

3.3 Sensitivity of eddy diffusivity estimates derived from simulated trajectories to lateral and temporal resolution

The spatial OGCM resolution determines to which degree eddies are explicitly resolved during the model simulation. The temporal model output resolution further restricts the scale of processes captured by offline simulated advective Lagrangian trajectories. In this section we quantify the sensitivity of the Lagrangian eddy diffusivity estimates to the temporal (5-day mean versus daily- and monthly- mean) model output resolution and spatial (1/10° versus 1/2°) OGCM resolution, whereby we focus on K_{inf}.

Sensitivity to the temporal model output resolution

In general, studies of oceanic features from the mesoscale to basin scales require a temporal model output resolution not longer than a few days. Using offline Lagrangian analyses within a high-resolution ocean model (1/10°), Qin et al. (2014) showed that the connectivity along six major currents does not significantly change for temporal resolutions between three-day and nine-day means. However, degradation in flow characteristics occurs at lower temporal resolutions, resulting in changed transit times and transports between selected upstream and downstream sections.

549 The comparison of our diffusivity estimates from SIMeddy-5d and SIMeddy-1d shows
550 that 5-day mean output is sufficient to capture the cumulative effect of eddies on particle
551 trajectories in the greater Agulhas system: using daily mean output does not substantially
552 change the spatial distribution (not shown) and magnitude of K_{inf} and the Lagrangian integral
553 time and length scales (Table 3).

554 SIMeddy-1m yields the same spatial pattern of K_{inf} as SIMeddy-5d (Figure 6b), but
555 with a generally reduced magnitude (exception: eddy diffusivities in the northern part of the
556 ACC and in near-coastal parts of the AR are increased compared to SIMeddy-5d), resulting in
557 lower spatial mean values, and a slightly smaller spatial variability (Figure 7, Table 3). Even
558 though eddy diffusivities are reduced, the spatial mean K_{inf} still reaches ~3.0 x 10^3 m^2 s^{-1}
559 (compared to ~3.4 x 10^3 m^2 s^{-1} in SIMeddy-5d). This suggests that monthly mean velocity
560 fields do capture a substantial amount of eddy variability – at least in the greater Agulhas
561 system. Yet, EKE is reduced by 26% (spatial average of 145 cm^2 s^{-2} in SIMeddy-1m
562 compared to 197 cm^2 s^{-2} in SIMeddy-5d), and average T_L and L_L are increased (Table 3). The
563 disproportional reduction of K_{inf} by only 12% again highlights that variability and changes in
564 K_{inf} cannot be directly explained by changes in EKE. The results further support the idea that
565 larger and more persistent eddy features are the dominant factors determining eddy
566 diffusivities (Wolfram et al. 2015).

567 These results agree with Qin et al. (2014), who showed that the connectivity transports
568 in the AC and AR revealed no significant changes for monthly mean fields compared to
569 three-day mean fields (in contrast to other investigated regions). Likewise, Biastoch et al.
570 (2015) and Cheng et al. (2016) reported interannual to decadal variability in Agulhas Leakage
571 transport to be captured by monthly-mean data. Yet, Qin et al. (2014) also noted that the mean
572 transit time for the AC does change significantly for monthly mean fields compared to three-
573 day mean fields. This can be explained by the fact that in the greater Agulhas system
574 connectivity transports, as eddy diffusivities, are dominated by the largest and most persistent

mesoscale features which are associated with the largest transports (and constitute some of the largest eddies of the world ocean), while transit time distributions are prone to be influenced by eddy variability at all scales.

Sensitivity to lateral OGCM resolution

By the criteria of Hallberg (2013), the ORCA05 model configuration is non-eddying in the extended Agulhas Current system, whereas INALT01 is eddy-resolving (cf. section 2.1). We already showed that SIMeddy-5d (as well as SIMeddy-1d and with slight restrictions also SIMeddy-1m) captures the general features of observed eddy diffusivities. In principle, eddy diffusivities (as well as EKE) obtained from non-eddying simulations should approach zero. In reality, the scale separation between eddies and mean flow is imperfect. Depending over which time and space scales the mean is defined, some lower frequency variance remains in the residual velocities and may lead to non-zero eddy diffusivity estimates even in so-called non-eddying ocean models. Furthermore, numerical noise introduces artificial high-frequency variability. Our analysis for SIMnoeddy-5d yields a spatial mean pseudo-Eulerian EKE of 53 $cm^2\ s^{-2}$ and corresponding K_{inf} of ~1.4 x 10^3 $m^2\ s^{-1}$ (Table 3). Hence, K_{inf} in SIMnoeddy-5d (Figure 6c) is on average 2.0 x 10^3 $m^2\ s^{-1}$ weaker than in SIMeddy-5d (cf. section 3.1), but still shows the rough spatial pattern from SIMeddy-5d and does not reach values close to zero. Again, the reduction in EKE (~73%) is larger than that in K_{inf} (~58%). The reduction of estimated lateral eddy diffusivities is consistent with the reduction of estimated isopycnal eddy diffusivities of ~50-60% reported by Wolfram et al. (2015) based on simulations with an idealized ocean basin at 32 km resolution compared to simulations at 8 km resolution (their Table 2).

Using the non-eddying OGCM configuration with online GM parameterization (SIMpareddy-5d) yields spatial mean pseudo-Eulerian EKE and eddy diffusivity estimates close to zero (Figure 6d). This is due to the fact that while parameterizing the advective effect of mesoscale eddies where there are not resolved by the model, GM also suppresses the

explicit generation of physical as well as numerical mesoscale variability (Hallberg 2013, cf. section 2.2).

In summary, Lagrangian trajectories simulated with the output from our coarse resolution OGCM configuration do not sufficiently capture the effect of mesoscale eddies on particle dispersal, which results in too low eddy diffusivity values compared to estimates based on observations and eddy-resolving model simulations. Lagragian eddy diffusivity estimates are further reduced by the employed GM parametrization. Nevertheless, for Lagrangian particle simulations the combined Eulerian and eddy-induced velocities from a model simulation with GM may be favored over velocities from coarse resolution model simulations without GM, since they are supposed to represent large-scale circulation patterns and the advective part of particle dispersal more realistically (cf. section 2.2). In order to capture the effect of mesoscale turbulence, one could fill the gap between coarse resolution simulations and observations/high-resolution simulations by stochastic Lagrangian parameterizations (cf. section 4).

4. Comparison with other eddy diffusivity estimates and implications for eddy parameterizations

Comparison with other eddy diffusivity estimates for the greater Agulhas system

Peng et al. (2015) derived Lagrangian eddy diffusivity estimates for the Indian Ocean from surface drifter data by using a binning technique similar to Zhurbas et al. (2014), but deriving diffusivities from the autocorrelation of residual velocities, which were calculated using the Gauss–Markov method (Lumpkin and Johnson 2013). They concluded that their diffusivity estimates (with seasonal effects removed) generally agree with the asymptotic estimates of Zhurbas et al. (2014), which can be confirmed by a closer inspection of their Figure 7 and our Figures 3g,h. In the region south of Madagascar our estimates for K_{inf} between 2.0×10^3 to

626 12.0 x 10^3 m^2 s^{-1} correspond well to their asymptotic minor principal component diffusivity
627 estimate κ_2 of 11.5 x 10^3 m^2 s^{-1} for region D7 (their table Table 2).

628 Our results also match the Osborn-Cox diffusivity calculated from the evolution of
629 passive tracers (simulated with surface velocities derived from AVISO sea-surface height
630 data) by Abernathey and Marshall (2013), who reported diffusivity values between 1.0 and
631 10.0 x 10^3 m^2 s^{-1} for the greater Agulhas system (their Figure 2). The overall agreement in
632 magnitude and spatial pattern of our particle- and their tracer-based diffusivity estimates is
633 encouraging. It supports the applicability of the results of Klocker et al. (2012b) and Wolfram
634 and Ringler (2017), showing that particle- and tracer-based diffusivities are similar in a
635 simple zonal channel flow, to the complex real oceanic circulation of the greater Agulhas
636 system.

637 ***Implications for stochastic parameterizations in offline trajectory calculations***

638 To derive more diffusive pathways capturing the effect of unresolved turbulence even from
639 coarse resolution OGCMs, stochastic Lagrangian parameterizations can be employed in
640 offline trajectory calculations (cf. section 1). However, it is still an open question how to
641 robustly specify an appropriate stochastic model and how to fit the associated parameters with
642 respect to the spatial and temporal resolution of any given Eulerian ocean model output.

643 Though we did not implement a stochastic parameterization here, our study reveals
644 important aspects to be considered: 1) Since asymptotic diffusive regimes could be identified
645 for different dynamic regimes in the greater Agulhas system, stochastic Lagrangian
646 parameterizations as described in Griffa et al. (1995) may indeed be appropriate to mimic the
647 effect of mesoscale turbulence in this region; 2) Stochastic Lagrangian parameterizations
648 should account for the spatial variability of the diffusivity parameter, which does not
649 necessarily scale with variability in EKE; 3) The choice of parameters in the stochastic
650 Lagrangian parameterizations should not only account for the horizontal (and temporal)

resolution of the underlying OGCM, but should also consider possible sub-grid scale parameterizations, such as GM.

Based on these considerations, we would like to emphasize that the application of a stochastic Lagrangian parameterization implies changing from a pure *Lagrangian analysis* of the Eulerian OGCM model output to a *Lagrangian modelling* approach of particle dispersion, which may break consistency with the underlying OGCM physics and thus – depending on the scientific question – may not always be desired.

Relation between Lagrangian eddy diffusivity estimates and diffusivity coefficients of OGCM diffusion parameterizations

The Lagrangian eddy diffusivity is a quantitative diagnostic for the cumulative effect of eddies on the Lagrangian dispersal and as such, it is used in this paper to assess simulated particle dispersal. However, others studies estimating Lagrangian eddy diffusivities from high-resolution OGCM output or drifter data are partially motivated by the desire to determine more realistic parameter values for Eulerian diffusion parameterizations in coarse-resolution OGCMs. It is therefore worthwhile to compare our Lagrangian diffusivity estimates with the diffusivity coefficients used in those parametrizations, such as the Redi coefficient (Redi 1982) A_{ht}. A_{ht} should quantify the effect of scales not resolved in the OGCM (i.e. variability occurring below 0.1° and 0.5° for INALT01 and ORCA05 experiments, respectively) on tracer mixing rates. Important for this context, Lagrangian eddy diffusivities derived from the respective OGCM represent the effect of the (fully or partially) resolved mesoscale on tracer mixing rates.

Following this reasoning, one would expect the difference in the Lagrangian eddy diffusivity estimates derived from a high-resolution OGCM experiment, e.g., SIMeddy-5d, and a coarse-resolution OGCM experiment, e.g., SIMnoeddy-5d, to be comparable in magnitude to the respective difference in the employed diffusivity coefficients. Both should be representative for the diffusive effect of mesoscale variability at horizontal scales between

677 0.1° and 0.5°. This is however not the case: The difference in the Lagrangian eddy
678 diffusivities exhibit a pronounced spatial variability at magnitudes $O(10^3)$ m^2 s^{-1}. Since A_{ht}
679 does not include spatial variability apart from its adaptation to the changing grid sizes, also
680 the difference in A_{ht} does not feature spatial variability. Even more strikingly, the difference
681 in A_{ht} only reaches magnitudes $O(10^2)$ m^2 s^{-1}.

682 This indicates that either the model coefficients are not chosen optimally, or, that
683 Eulerian diffusivity coefficients and Lagrangian eddy diffusivity estimates are two measures
684 that cannot be easily compared.

685 One could argue that Lagrangian eddy diffusivity estimates derived from drifter data
686 quantify the rate of lateral dispersal in the surface mixed layer, whereas most modern ocean
687 models, as those employed here, use isopycnal diffusivities for their sub-grid scale
688 parametrizations. Yet, mesoscale eddies mix tracers along isopycnals and horizontally at the
689 sea surface (Treguier et al. 1997; Abernathey et al. 2013), so that the lateral eddy diffusivities
690 estimated from GDP data and our simulated drifter trajectories can be treated as eddy
691 diffusivity in the surface mixed layer. However, model diffusivities have to be tuned not only
692 with respect to physical, but also with respect to numerical considerations. Profound
693 simplifications in the OGCM diffusion parametrization may further inhibit a direct relation
694 between Eulerian diffusivity coefficients and Lagrangian eddy diffusivity estimates. Also to
695 consider, as already stated by Rypina et al. (2016), Lagrangian diffusivity estimates constitute
696 non-local measures, while the diffusivity coefficient for the sub-grid scale parameterization
697 should represent the local effect of eddies. Finally, keeping in mind the challenges of
698 Lagrangian eddy diffusivity estimation, such as removing the mean flow effect and capturing
699 truly asymptotic regimes, Lagrangian eddy diffusivity estimates may not exclusively quantify
700 the impact of mesoscale eddies but may be additionally influenced by methodological
701 choices. Therefore, tuning coarse-resolution OGCM Eulerian eddy diffusivity coefficients

based on Lagrangian eddy diffusivities estimated from high-resolution models or observations remains an outstanding issue which needs to be further addressed in more dedicated studies.

5. Conclusions

In this study we assessed spatially variable near-surface lateral (mesoscale) eddy diffusivity estimates obtained from both simulated Lagrangian trajectories and real drifter data for the greater Agulhas system following the approach of Zhurbas et al. (2014). Answering the three questions outlined in section 1 we showed that in this region:

(1) Using 5-day mean velocity fields from the eddy-resolving ocean model configuration INALT01, asymptotic diffusive regimes could be identified for dynamically different sites, some of which exhibit strong suppression of eddy mixing by mean flow.

(2) The Lagrangian model-based eddy diffusivity estimates agree in pattern and magnitude with the observational-based estimates from Zhurbas et al. (2014), and are also comparable to the tracer-based eddy diffusivity estimates provided by Abernathey and Marshall (2013).

(3a) Using monthly-mean velocity output decreases the EKE, but decreases eddy diffusivity estimates disproportionally less, supporting the idea that larger and more persistent eddy features are the dominant factors determining eddy diffusivities (cf. Wolfram et al. (2015)).

(3b) Using 5-day mean velocity fields from the non-eddying ocean model configuration ORCA05 greatly reduces Lagrangian lateral eddy diffusivities; if a GM parameterization is employed, diffusivities further reduce to values close to zero.

These results suggest that when employing a stochastic Lagrangian parameterization to derive more diffusive trajectories from coarse-resolution model output – in particular for large-scale applications – one should consider the spatial variability of the diffusivity

parameter, which does not necessarily scale with variability in EKE, as well as possible sub-grid scale parameterizations such as GM.

Acknowledgements

OGCM experiments and trajectory simulations were performed at High Performance Computing Centers in Stuttgart (HLRS), Hannover (HLRN) and at the Christian-Albrechts-Universität zu Kiel. OGCM code and data are available upon request from the corresponding author. For reproducibility of all result figures in this study, respective data is available at http://data.geomar.de. The project received funding by the Cluster of Excellence 80 "The Future Ocean" within the framework of the Excellence Initiative by the Deutsche Forschungsgemeinschaft (DFG) on behalf of the German federal and state governments (Siren Rühs, Grant CP1412), by the German Federal Ministry of Education and Research (BMBF) (Arne Biastoch, Grant 03F0750A of the SPACES-AGULHAS project), and by the Helmholtz Association and the GEOMAR Helmholtz Centre for Ocean Research Kiel (Jonathan V. Durgadoo, Grant IV014/GH018). Victor Zhurbas was supported by the Russian Science Foundation (Grant 14-50-00095) and the Russian Foundation for Basic Research (Grant18-05-00278). The authors further wish to acknowledge the DRAKKAR group for support in model development and two anonymous reviewers for their insightful comments which helped to improve this manuscript.

APPENDIX A

Details of the eddy diffusivity estimation – smoothing choices and deviation from the original Zhurbas et al. (2014) approach

We followed the approach by Zhurbas et al. (2014) in all fundamental steps summarized in Figure 8, which were already introduced by Oh et al. (2000), including the smoothing

approaches adjusted to the spatial-temporal coverage of drifter data. Due to the increase of the sampling error with increasing time lag (Davis 1991b), a time-dependent finite differencing was applied to obtain $k_{jk}^{disp}(x,t)$, and the tensor components $k_{jk}(x,t)$ and $s_{jk}(x,t)$ were low-pass filtered with a cosine filter and time-dependent filter window length. The time increment δt was chosen to equal the filter window $[t-0.2t, t+0.2t]$. Further details can be found in Oh et al. (2000), Zhurbas and Oh (2004), and Zhurbas et al. (2014). Note that simulated drifter trajectories were processed identical to the drifter data for comparability reasons. For a pure model study with a very large number of trajectories less smoothing and non-overlapping bins may be sufficient and preferred, as indicated by Figure 9: The asymptotic diffusivity estimates inferred from SIMeddy-5d hardly change when removing the time-dependent filtering and differencing, and also show only small changes when changing to non-overlapping 2° x 2° bins.

We deviated from the original Zhurbas et al. (2014) approach by slightly altering the quality control of drifter data to allow for speeds until 3 m s^{-1} (instead of removing data with speeds > 2 m s^{-1}), since in the region of interest velocities reaching (exceeding) 2 m s^{-1} were reported from observations (and are apparent in the modeled velocity fields). We were further able to increase the number of considered pseudo-tracks for large time lags by extending the area over which trajectories were sampled for a certain bin (also necessary due to the very high local current velocities and thus large dispersion due to mean currents). Finally, we fixed a slight inconsistency in the estimation of K_{max} which previously only considered time lags until 10 days (occasionally leading to $K_{inf} > K_{max}$).

773 **References**

774 Abernathey, R., D. Ferreira, and A. Klocker, 2013: Diagnostics of isopycnal mixing in a
775 circumpolar channel. *Ocean Model.*, **72**, 1–16, doi:10.1016/j.ocemod.2013.07.004.
776 Abernathey, R. P., and J. Marshall, 2013: Global surface eddy diffusivities derived from
777 satellite altimetry. *J. Geophys. Res. Ocean.*, **118**, 901–916, doi:10.1002/jgrc.20066.
778 Arakawa, A., and Y.-J. G. Hsu, 1990: Energy Conserving and Potential-Enstrophy
779 Dissipating Schemes for the Shallow Water Equations. *Mon. Weather Rev.*, **118**, 1960–
780 1969.
781 Barnier, B., and Coauthors, 2014: DRAKKAR: developing high resolution ocean components
782 for European Earth system models. *CLIVAR Exch.*, **65**–**19**, 18–21.
783 Bates, M., R. Tulloch, J. Marshall, and R. Ferrari, 2014: Rationalizing the Spatial Distribution
784 of Mesoscale Eddy Diffusivity in Terms of Mixing Length Theory. *J. Phys. Oceanogr.*,
785 **44**, 1523–1540, doi:10.1175/JPO-D-13-0130.1.
786 Bauer, S., M. S. Swenson, and A. Griffa, 2002: Eddy mean flow decomposition and eddy
787 diffusivity estimates in the tropical Pacific Ocean: 2. Results. *J. Geophys. Res.*, **107**,
788 3154, doi:10.1029/2000JC000613.
789 Beal, L. M., W. P. M. de Ruijter, A. Biastoch, R. Zahn, and S. W. G. 136, 2011: On the role
790 of the Agulhas system in ocean circulation and climate. *Nature*, **472**, 429–436,
791 doi:10.1038/nature09983.
792 Berloff, P. S., and J. C. McWilliams, 2002: Material Transport in Oceanic Gyres. Part II:
793 Hierarchy of Stochastic Models. *J. Phys. Oceanogr.*, **32**, 797–830, doi:10.1175/1520-
794 0485(2002)032<0764:MTIOGP>2.0.CO;2.
795 Biastoch, A., C. W. Böning, and J. R. E. Lutjeharms, 2008a: Agulhas leakage dynamics
796 affects decadal variability in Atlantic overturning circulation. *Nature*, **456**, 489–492,
797 doi:10.1038/nature07426.
798 ——, J. R. E. Lutjeharms, C. W. Böning, and M. Scheinert, 2008b: Mesoscale perturbations

799 control inter-ocean exchange south of Africa. *Geophys. Res. Lett.*, **35**, L20602,
800 doi:10.1029/2008GL035132.
801 ——, J. V. Durgadoo, A. K. Morrison, E. van Sebille, W. Weijer, and S. M. Griffies, 2015:
802 Atlantic multi-decadal oscillation covaries with Agulhas leakage. *Nat. Commun.*, **6**,
803 10082, doi:10.1038/ncomms10082.
804 Blanke, B., and S. Raynaud, 1997: Kinematics of the Pacific Equatorial Undercurrent: An
805 Eulerian and Lagrangian Approach from GCM Results. *J. Phys. Oceanogr.*, **27**, 1038–
806 1053, doi:10.1175/1520-0485(1997)027<1038:KOTPEU>2.0.CO;2.
807 ——, S. Speich, G. Madec, and K. Döös, 2001: A Global Diagnostic of Interocean Mass
808 Transfers. *J. Phys. Oceanogr.*, **31**, 1623–1632, doi:10.1175/1520-
809 0485(2001)031<1623:AGDOIM>2.0.CO;2.
810 ——, S. Speich, G. Madec, and R. Maugé, 2002: A global diagnostic of interior ocean
811 ventilation. *Geophys. Res. Lett.*, **29**, 1267, doi:10.1029/2001GL013727.
812 Boebel, O., T. Rossby, J. Lutjeharms, W. Zenk, and C. Barron, 2003: Path and variability of
813 the Agulhas Return Current. *Deep. Res. Part II Top. Stud. Oceanogr.*, **50**, 35–56,
814 doi:10.1016/S0967-0645(02)00377-6.
815 Chelton, D. B., M. G. Schlax, and R. M. Samelson, 2011: Global observations of nonlinear
816 mesoscale eddies. *Prog. Oceanogr.*, **91**, 167–216, doi:10.1016/j.pocean.2011.01.002.
817 Chen, R., J. L. McClean, S. T. Gille, and A. Griesel, 2014: Isopycnal Eddy Diffusivities and
818 Critical Layers in the Kuroshio Extension from an Eddying Ocean Model. *J. Phys.*
819 *Oceanogr.*, **44**, 2191–2211, doi:10.1175/JPO-D-13-0258.1.
820 Cheng, Y., D. Putrasahan, L. Beal, and B. Kirtman, 2016: Quantifying Agulhas Leakage in a
821 High-Resolution Climate Model. *J. Clim.*, **29**, 6881–6892, doi:10.1175/JCLI-D-15-
822 0568.1.
823 Cronin, M. F., T. Tozuka, A. Biastoch, J. V. Durgadoo, and L. M. Beal, 2013: Prevalence of
824 strong bottom currents in the greater Agulhas system. *Geophys. Res. Lett.*, **40**, 1772–

825 1776, doi:10.1002/grl.50400.
826 Danabasoglu, G., and Coauthors, 2014: North Atlantic simulations in Coordinated Ocean-ice
827 Reference Experiments phase II (CORE-II). Part I: Mean states. *Ocean Model.*, **73**, 76–
828 107, doi:10.1016/j.ocemod.2013.10.005.
829 Davis, R. E., 1991a: Lagrangian Ocean Studies. *Annu. Rev. Fluid Mech.*, **23**, 43–64,
830 doi:10.1146/annurev.fluid.23.1.43.
831 ——, 1991b: Observing the general circulation with floats. *Deep Sea Res. Part A. Oceanogr.*
832 *Res. Pap.*, **38**, S531–S571, doi:10.1016/S0198-0149(12)80023-9.
833 Dencausse, G., M. Arhan, and S. Speich, 2010: Routes of Agulhas rings in the southeastern
834 Cape Basin. *Deep Sea Res. Part I Oceanogr. Res. Pap.*, **57**, 1406–1421,
835 doi:10.1016/j.dsr.2010.07.008.
836 De Dominicis, M., G. Leuzzi, P. Monti, N. Pinardi, and P. M. Poulain, 2012: Eddy diffusivity
837 derived from drifter data for dispersion model applications. *Ocean Dyn.*, **62**, 1381–1398,
838 doi:10.1007/s10236-012-0564-2.
839 Döös, K., V. Rupolo, and L. Brodeau, 2011: Dispersion of surface drifters and model-
840 simulated trajectories. *Ocean Model.*, **39**, 301–310, doi:10.1016/j.ocemod.2011.05.005.
841 ——, J. Nilsson, J. Nycander, L. Brodeau, and M. Ballarotta, 2012: The World Ocean
842 Thermohaline Circulation. *J. Phys. Oceanogr.*, **42**, 1445–1460, doi:10.1175/JPO-D-11-
843 0163.1.
844 Drijfhout, S. S., P. De Vries, K. Doos, and A. C. Coward, 2003: Impact of Eddy-Induced
845 Transport on the Lagrangian Structure of the Upper Branch of the Thermohaline
846 Circulation. *J. Phys. Ocean.*, **33**, 2141–2155, doi:10.1175/1520-
847 0485(2003)033<2141:IOETOT>2.0.CO;2.
848 Durgadoo, J. V., B. R. Loveday, C. J. C. Reason, P. Penven, and A. Biastoch, 2013: Agulhas
849 Leakage Predominantly Responds to the Southern Hemisphere Westerlies. *J. Phys.*
850 *Oceanogr.*, **43**, 2113–2131, doi:10.1175/JPO-D-13-047.1.

851 ——, S. Rühs, A. Biastoch, and C. W. B. Böning, 2017: Indian Ocean sources of Agulhas
852 leakage. *J. Geophys. Res. Ocean.*, **122**, 3481–3499, doi:10.1002/2016JC012676.
853 Eden, C., and H. Dietze, 2009: Effects of mesoscale eddy/wind interactions on biological new
854 production and eddy kinetic energy. *J. Geophys. Res. Ocean.*, **114**, C05023,
855 doi:10.1029/2008JC005129.
856 Gary, S. F., M. S. Lozier, Y.-O. Kwon, and J. J. Park, 2014: The Fate of North Atlantic
857 Subtropical Mode Water in the FLAME Model. *J. Phys. Oceanogr.*, **44**, 1354–1371,
858 doi:10.1175/JPO-D-13-0202.1.
859 Gent, P. R., 2011: The Gent-McWilliams parameterization: 20/20 hindsight. *Ocean Model.*,
860 **39**, 2–9, doi:10.1016/j.ocemod.2010.08.002.
861 ——, and J. C. Mcwilliams, 1990: Isopycnal Mixing in Ocean Circulation Models. *J. Phys.*
862 *Oceanogr.*, **20**, 150–155, doi:10.1175/1520-0485(1990)020<0150:IMIOCM>2.0.CO;2.
863 ——, J. Willebrand, T. J. McDougall, and J. C. McWilliams, 1995: Parameterizing Eddy-
864 Induced Tracer Transports in Ocean Circulation Models. *J. Phys. Oceanogr.*, **25**, 463–
865 474, doi:10.1175/1520-0485(1995)025<0463:PEITTI>2.0.CO;2.
866 Griesel, A., S. T. Gille, J. Sprintall, J. L. McClean, J. H. LaCasce, and M. E. Maltrud, 2010:
867 Isopycnal diffusivities in the Antarctic Circumpolar Current inferred from Lagrangian
868 floats in an eddying model. *J. Geophys. Res. Ocean.*, **115**, C06006,
869 doi:10.1029/2009JC005821.
870 ——, J. L. McClean, S. T. Gille, J. Sprintall, and C. Eden, 2014: Eulerian and Lagrangian
871 Isopycnal Eddy Diffusivities in the Southern Ocean of an Eddying Model. *J. Phys.*
872 *Oceanogr.*, **44**, 644–661, doi:10.1175/JPO-D-13-039.1.
873 Griffa, A., 1996: Applications of stochastic particle models to oceanographic problems.
874 *Stochastic Modelling in Physical Oceanography*, R.J. Adler, P. Müller, and B.L.
875 Rozowskii, Eds., Birkhäuser, Boston, 113–140.
876 ——, K. Owens, L. Piterbarg, and B. Rozovskii, 1995: Estimates of turbulence parameters

877 from Lagrangian data using a stochastic particle model. *J. Mar. Res.*, **53**, 371–401,
878 doi:10.1357/0022240953213151.
879 Griffies, S., and Coauthors, 2009: Coordinated Ocean-ice Reference Experiments (COREs).
880 *Ocean Model.*, **26**, 1–46, doi:10.1016/j.ocemod.2008.08.007.
881 Hallberg, R., 2013: Using a resolution function to regulate parameterizations of oceanic
882 mesoscale eddy effects. *Ocean Model.*, **72**, 92–103, doi:10.1016/j.ocemod.2013.08.007.
883 Hansen, D. V., and P.-M. Poulain, 1996: Quality Control and Interpolations of WOCE-TOGA
884 Drifter Data. *J. Atmos. Ocean. Technol.*, **13**, 900–909, doi:10.1175/1520-0426.
885 Keating, S. R., K. S. Smith, and P. R. Kramer, 2011: Diagnosing Lateral Mixing in the Upper
886 Ocean with Virtual Tracers: Spatial and Temporal Resolution Dependence. *J. Phys.*
887 *Oceanogr.*, **41**, 1512–1534, doi:10.1175/2011JPO4580.1.
888 Klocker, A., R. Ferrari, and J. H. LaCasce, 2012a: Estimating Suppression of Eddy Mixing by
889 Mean Flows. *J. Phys. Oceanogr.*, **42**, 1566–1576, doi:10.1175/JPO-D-11-0205.1.
890 ——, ——, ——, and S. T. Merrifield, 2012b: Reconciling float-based and tracer-based
891 estimates of lateral diffusivities. *J. Mar. Res.*, **70**, 569–602,
892 doi:10.1357/002224012805262743.
893 Koszalka, I. M., and J. H. Lacasce, 2010: Lagrangian analysis by clustering. *Ocean Dyn.*, **60**,
894 957–972, doi:10.1007/s10236-010-0306-2.
895 ——, J. H. LaCasce, M. Andersson, K. A. Orvik, and C. Mauritzen, 2011: Surface circulation
896 in the Nordic Seas from clustered drifters. *Deep. Res. Part I Oceanogr. Res. Pap.*, **58**,
897 468–485, doi:10.1016/j.dsr.2011.01.007.
898 ——, T. W. N. Haine, and M. G. Magaldi, 2013a: Fates and Travel Times of Denmark Strait
899 Overflow Water in the Irminger Basin. *J. Phys. Oceanogr.*, **43**, 2611–2628,
900 doi:10.1175/JPO-D-13-023.1.
901 ——, J. H. LaCasce, and C. Mauritzen, 2013b: In pursuit of anomalies - Analyzing the
902 poleward transport of Atlantic Water with surface drifters. *Deep. Res. Part II Top. Stud.*

903 *Oceanogr.*, **85**, 96–108, doi:10.1016/j.dsr2.2012.07.035.
904 Krauss, W., and C. W. Böning, 1987: Lagrangian properties of eddy fields in the northern
905 North Atlantic as deduced from satellite-tracked buoys. *J. Mar. Res.*, **45**, 259–291,
906 doi:10.1357/002224087788401142.
907 LaCasce, J. H., 2008a: Statistics from Lagrangian observations. *Prog. Oceanogr.*, **77**, 1–29,
908 doi:10.1016/j.pocean.2008.02.002.
909 ——, 2008b: Statistics from Lagrangian observations. *Prog. Oceanogr.*, **77**, 1–29,
910 doi:10.1016/j.pocean.2008.02.002.
911 Large, W. G., and S. G. Yeager, 2008: The global climatology of an interannually varying
912 air–sea flux data set. *Clim. Dyn.*, **33**, 341–364, doi:10.1007/s00382-008-0441-3.
913 Laurindo, L. C., A. J. Mariano, and R. Lumpkin, 2017: An improved near-surface velocity
914 climatology for the global ocean from drifter observations. *Deep. Res. Part I Oceanogr.*
915 *Res. Pap.*, **124**, 73–92, doi:10.1016/j.dsr.2017.04.009.
916 Lique, C., A. M. Treguier, B. Blanke, and N. Grima, 2010: On the origins of water masses
917 exported along both sides of Greenland: A Lagrangian model analysis. *J. Geophys. Res.*
918 *Ocean.*, **115**, C05019, doi:10.1029/2009JC005316.
919 Loveday, B. R., J. V. Durgadoo, C. J. C. Reason, A. Biastoch, and P. Penven, 2014:
920 Decoupling of the Agulhas Leakage from the Agulhas Current. *J. Phys. Oceanogr.*, **44**,
921 1776–1797, doi:10.1175/JPO-D-13-093.1.
922 Lübbecke, J. F., J. V. Durgadoo, and A. Biastoch, 2015: Contribution of Increased Agulhas
923 Leakage to Tropical Atlantic Warming. *J. Clim.*, **28**, 9697–9706, doi:10.1175/JCLI-D-
924 15-0258.1.
925 Lumpkin, R., and P. Flament, 2001: Lagrangian statistics in the central North Pacific. *J. Mar.*
926 *Syst.*, **29**, 141–155, doi:10.1016/S0924-7963(01)00014-8.
927 ——, and S. L. Garzoli, 2005: Near-surface circulation in the Tropical Atlantic Ocean. *Deep*
928 *Sea Res. Part I Oceanogr. Res. Pap.*, **52**, 495–518, doi:10.1016/j.dsr.2004.09.001.

929 ——, and M. Pazos, 2007: Measuring surface currents with Surface Velocity Program
930 drifters: the instrument, its data, and some recent results. *Lagrangian Analysis and*
931 *Prediction of Coastal and Ocean Dynamics*, Cambridge University Press, Cambridge,
932 39–67.
933 ——, and G. C. Johnson, 2013: Global ocean surface velocities from drifters: Mean, variance,
934 El Nino-Southern Oscillation response, and seasonal cycle. *J. Geophys. Res. Ocean.*,
935 **118**, 2992–3006, doi:10.1002/jgrc.20210.
936 ——, S. A. Grodsky, L. Centurioni, M. H. Rio, J. A. Carton, and D. Lee, 2013: Removing
937 Spurious Low-Frequency Variability in Drifter Velocities. *J. Atmos. Ocean. Technol.*,
938 **30**, 353–360, doi:10.1175/JTECH-D-12-00139.1.
939 ——, T. Özgökmen, and L. Centurioni, 2017: Advances in the Application of Surface
940 Drifters. *Ann. Rev. Mar. Sci.*, **9**, 59–81, doi:10.1146/annurev-marine-010816-060641.
941 Lutjeharms, J. R. E., 2006: *The Agulhas Current*. Springer, Berlin, 329 pp.
942 ——, 2007: Three decades of research on the greater Agulhas Current. *Ocean Sci.*, **3**, 129–
943 147, doi:10.5194/os-3-129-2007.
944 ——, and I. J. Ansorge, 2001: The Agulhas Return Current. *J. Mar. Syst.*, **30**, 115–138,
945 doi:10.1016/S0924-7963(01)00041-0.
946 Madec, G., 2008: NEMO ocean engine. *Note du Pole de modelisation*, Institut Pierre-Simon
947 Laplace (IPSL), France, No 27.
948 McClean, J. L., P. M. Poulain, J. W. Pelton, and M. E. Maltrud, 2002: Eulerian and
949 Lagrangian statistics from surface drifters and a high-resolution POP simulation in the
950 North Atlantic. *J. Phys. Oceanogr.*, **32**, 2472–2491, doi:10.1175/1520-0485-32.9.2472.
951 Mesinger, F., and A. Arakawa, 1976: Numerical methods used in atmospheric models. *Glob.*
952 *Atmos. Res. Progr. World Meteorol. Organ.*, **1**, 1–65.
953 Monti, P., and G. Leuzzi, 2010: Lagrangian models of dispersion in marine environment.
954 *Environ. Fluid Mech.*, **10**, 637–656, doi:10.1007/s10652-010-9184-x.

Oh, I. S., V. Zhurbas, and W. Park, 2000: Estimating horizontal diffusivity in the East Sea (Sea of Japan) and the northwest Pacific from satellite-tracked drifter data. *J. Geophys. Res.*, **105**, 6483–6492, doi:10.1029/2000JC900002.

Peng, S., Y.-K. Qian, R. Lumpkin, P. Li, D. Wang, and Y. Du, 2015: Characteristics of the Near-Surface Currents in the Indian Ocean as Deduced from Satellite-Tracked Surface Drifters. Part II: Lagrangian Statistics. *J. Phys. Oceanogr.*, **45**, 459–477, doi:10.1175/JPO-D-14-0049.1.

Poulain, P.-M., 2001: Adriatic sea surface circulation as derived from drifters data between 1990 and 1999. *J. Mar. Syst.*, **29**, 3–32, doi:10.1016/S0924-7963(01)00007-0.

——, R. Gerin, E. Mauri, and R. Pennel, 2009: Wind Effects on Drogued and Undrogued Drifters in the Eastern Mediterranean. *J. Atmos. Ocean. Technol.*, **26**, 1144–1156, doi:10.1175/2008JTECHO618.1.

Qin, X., E. van Sebille, and A. Sen Gupta, 2014: Quantification of errors induced by temporal resolution on Lagrangian particles in an eddy-resolving model. *Ocean Model.*, **76**, 20–30, doi:10.1016/j.ocemod.2014.02.002.

Redi, M. H., 1982: Oceanic Isopycnal Mixing by Coordinate Rotation. *J. Phys. Oceanogr.*, **12**, 1154–1158, doi:10.1175/1520-0485(1982)012<1154:OIMBCR>2.0.CO;2.

Rieck, J. K., C. W. Böning, R. J. Greatbatch, and M. Scheinert, 2015: Seasonal variability of eddy kinetic energy in a global high-resolution ocean model. *Geophys. Res. Lett.*, **42**, 9379–9386, doi:10.1002/2015GL066152.

Rühs, S., J. V. Durgadoo, E. Behrens, and A. Biastoch, 2013: Advective timescales and pathways of Agulhas leakage. *Geophys. Res. Lett.*, **40**, 3997–4000, doi:10.1002/grl.50782.

Rypina, I. I., I. Kamenkovich, P. Berloff, and L. J. Pratt, 2012: Eddy-Induced Particle Dispersion in the Near-Surface North Atlantic. *J. Phys. Oceanogr.*, **42**, 2206–2228, doi:10.1175/JPO-D-11-0191.1.

981 ——, A. Kirincich, S. Lentz, and M. Sundermeyer, 2016: Investigating the Eddy Diffusivity
982 Concept in the Coastal Ocean. *J. Phys. Oceanogr.*, **46**, 2201–2218, doi:10.1175/JPO-D-
983 16-0020.1.
984 Sallée, J. B., K. Speer, R. Morrow, and R. Lumpkin, 2008: An estimate of Lagrangian eddy
985 statistics and diffusion in the mixed layer of the Southern Ocean. *J. Mar. Res.*, **66**, 441–
986 463, doi:10.1357/002224008787157458.
987 Schouten, M. W., W. P. M. de Ruijter, P. J. van Leeuwen, and J. R. E. Lutjeharms, 2000:
988 Translation, decay and splitting of Agulhas rings in the southeastern Atlantic Ocean. *J.*
989 *Geophys. Res.*, **105**, 21913–21925, doi:10.1029/1999JC000046.
990 ——, W. P. M. de Ruijter, and P. J. van Leeuwen, 2002: Upstream control of Agulhas Ring
991 shedding. *J. Geophys. Res.*, **107**, 1–11, doi:10.1029/2001JC000804.
992 van Sebille, E., P. J. van Leeuwen, A. Biastoch, C. N. Barron, and W. P. M. de Ruijter, 2009:
993 Lagrangian validation of numerical drifter trajectories using drifting buoys: Application
994 to the Agulhas system. *Ocean Model.*, **29**, 269–276, doi:10.1016/j.ocemod.2009.05.005.
995 ——, L. M. Beal, and W. E. Johns, 2011: Advective Time Scales of Agulhas Leakage to the
996 North Atlantic in Surface Drifter Observations and the 3D OFES Model. *J. Phys.*
997 *Oceanogr.*, **41**, 1026–1034, doi:10.1175/201.
998 ——, P. Spence, M. R. Mazloff, M. H. England, S. R. Rintoul, and O. a. Saenko, 2013:
999 Abyssal connections of Antarctic Bottom Water in a Southern Ocean State Estimate.
1000 *Geophys. Res. Lett.*, **40**, 2177–2182, doi:10.1002/grl.50483.
1001 ——, J. Sprintall, F. U. Schwarzkopf, A. Sen Gupta, A. Santoso, M. H. England, A. Biastoch,
1002 and C. W. Böning, 2014: Pacific-to-Indian Ocean connectivity: Tasman leakage,
1003 Indonesian Throughflow, and the role of ENSO. *J. Geophys. Res. Ocean.*, **119**, 1365–
1004 1382, doi:10.1002/2013JC009525.
1005 Speich, S., B. Blanke, and G. Madec, 2001: Warm and cold water routes of an OGCM
1006 thermohaline Conveyor Belt. *Geophys. Res. Lett.*, **28**, 311–314,

doi:10.1029/2000GL011748.

Swenson, M. S., and P. P. Niiler, 1996: Statistical analysis of the surface circulation of the California Current. *J. Geophys. Res.*, **101**, 22631–22645.

Taylor, G. I., 1922: Diffusion by Continuous Movements. *Proc. London Math. Soc.*, **s2-20**, 196–212, doi:10.1112/plms/s2-20.1.196.

The DRAKKAR Group, 2007: Eddy-permitting ocean circulation hindcasts of past decades. *Clivar Exch.*, **12**, 8–11.

Treguier, A. M., I. M. Held, and V. D. Larichev, 1997: Parameterization of Quasigeostrophic Eddies in Primitive Equation Ocean Models. *J. Phys. Oceanogr.*, **27**, 567–580, doi:10.1175/1520-0485(1997)027<0567:POQEIP>2.0.CO;2.

Uchida, T., R. Abernathey, and S. Smith, 2017: Seasonality of eddy kinetic energy in an eddy permitting global climate model. *Ocean Model.*, **118**, 41–58, doi:10.1016/J.OCEMOD.2017.08.006.

de Verdiere, A. C., 1983: Lagrangian eddy statistics from surface drifters in the eastern North Atlantic. *J. Mar. Res.*, **41**, 375–398, doi:10.1357/002224083788519713.

Wolfram, P. J., and T. D. Ringler, 2017a: Quantifying Residual, Eddy, and Mean Flow Effects on Mixing in an Idealized Circumpolar Current. *J. Phys. Oceanogr.*, **47**, 1897–1920, doi:10.1175/JPO-D-16-0101.1.

——, and ——, 2017b: Computing eddy-driven effective diffusivity using Lagrangian particles. *Ocean Model.*, **118**, 94–106, doi:10.1016/J.OCEMOD.2017.08.008.

——, ——, M. E. Maltrud, D. W. Jacobsen, and M. R. Petersen, 2015: Diagnosing Isopycnal Diffusivity in an Eddying, Idealized Midlatitude Ocean Basin via Lagrangian, in Situ, Global, High-Performance Particle Tracking (LIGHT). *J. Phys. Oceanogr.*, **45**, 2114–2133, doi:10.1175/JPO-D-14-0260.1.

Zalesak, S. T., 1979: Fully multidimensional flux-corrected transport algorithms for fluids. *J. Comput. Phys.*, **31**, 335–362, doi:10.1016/0021-9991(79)90051-2.

1033 Zhurbas, V., and I. S. Oh, 2004: Drifter-derived maps of lateral diffusivity in the Pacific and
1034 Atlantic Oceans in relation to surface circulation patterns. *J. Geophys. Res. C Ocean.*,
1035 **109**, C05015, doi:10.1029/2003JC002241.
1036 ——, D. Lyzhkov, and N. Kuzmina, 2014: Drifter-derived estimates of lateral eddy
1037 diffusivity in the World Ocean with emphasis on the Indian Ocean and problems of
1038 parameterisation. *Deep Sea Res. Part I Oceanogr. Res. Pap.*, **83**, 1–11,
1039 doi:10.1016/j.dsr.2013.09.001.
1040

Tables

Lagrangian experiment	OGCM configuration /simulation	horizontal resolution	Sub-grid scale parameterizations $[A_{ht0}] = m^2 s^{-1}$ $[A_{hm0}] = m^4 s^{-1}$	spin-up	forcing type/ period	temporal output resolution/period
SIMeddy-1d	INALT01/ KJD308	- base model: 1/2° - nest: 1/10°	-base model: A_{ht0}: 600 A_{hm0}: $-12x10^{11}$ -nest: A_{ht0}: 200 A_{hm0}: $-2.125x10^{10}$	- base model: forcing 1978-1997 (JD305) - nest: no spin-up, initialized with base model fields	hindcast/ 1948-2007 (1-day mean fields only between 1995-2007)	1-day mean/ 1996-2007
SIMeddy-5d						5-day mean/ 1996-2007
SIMeddy-1m						monthly mean/ 1996-2007
SIMeddy-5d-clim	INALT01/ KJD309				climatological/ 60 years	5day mean/ year 49-60
SIMnoeddy-5d	ORCA05/ JD308	globally 1/2°	A_{ht0}: 600 A_{hm0}: $-12x10^{11}$	forcing 1978-1997 (JD305)	hindcast/ 1948-2007	5-day mean/ 1996-2007
SIMpareddy-5d	ORCA05 JD409		A_{ht0}: 600 A_{hm0}: $-12x10^{11}$ + GM	forcing 1978-1997 (JD405)	climatological/ 60 years	5-day mean/ year 49-60

Table 1: Summary of the global ocean general circulation model (OGCM) simulations, which provided the velocity fields used for 6 Lagrangian experiments performed in this study. All OGCM simulations used a Laplacian iso-neutral diffusion of tracers (with different values for the isopycnal diffusivity coefficient A_{ht0}) and a bi-Laplacian lateral diffusion of momentum (with different values for the horizontal viscosity coefficient A_{hm0}).

Region	Lagrangian experiment	Speed in $cm\ s^{-1}$	EKE in $cm^2\ s^{-2}$	Kinf in $10^3\ m^2\ s^{-1}$			Kmax in $10^3\ m^2\ s^{-1}$			T_L in days	L_L in km
				K	Kdav	Kdisp	K	Kdav	Kdisp		
Eastern South Atlantic	SIMeddy-5d	4	15	1.46	1.51	1.41	1.53	1.59	1.47	11.6	38.2
Gyre (eSAG; 24°S, 5°W)	OBS	5	42	1.95	2.02	1.89	1.96	2.03	1.91	5.4	30.2
Agulhas Return Current	SIMeddy-5d	17	482	3.04	3.88	2.20	12.20	12.30	12.50	0.7	13.9
(ARC; 40°S, 35°E)	OBS	15	607	4.12	4.58	3.67	8.87	8.99	8.75	0.8	16.7
Agulhas Retroflection	SIMeddy-5d	6	1218	11.20	14.40	8.07	21.80	22.30	21.70	1.1	32.0
(AR; 40°S, 17°E)	OBS	12	1266	9.81	7.75	11.90	19.20	18.30	20.10	0.9	27.6
Agulhas Current	SIMeddy-5d	16	193	5.25	3.40	7.10	5.31	4.23	7.15	3.2	38.2
(AC; 32°S, 31°E)	OBS	24	458	4.43	3.70	5.17	8.07	9.54	8.34	1.1	20.7

Table 2: Statistics for 4 selected 5° x 5° bins centered on the listed coordinates: Pseudo-Eulerian mean speed and mean eddy kinetic energy (EKE), as well as asymptotic (K_{inf}) and maximum (K_{max}) near-surface lateral eddy diffusivity estimates, and Lagrangian integral time (T_L) and length (L_L) scales obtained from surface drifter data (OBS) and Lagrangian experiment SIMeddy-5d**.**

Lagrangian experiment	Speed in $cm\ s^{-1}$	EKE in $cm^2\ s^{-2}$	Kinf in $10^3\ m^2\ s^{-1}$			Kmax in $10^3\ m^2\ s^{-1}$			T_L in days	L_L in km
			K	Kdav	Kdisp	K	Kdav	Kdisp		
OBS	11	307	4.09	3.87	4.33	6.03	5.94	6.58	2.1	24.6
SIMeddy-1d	7	200	3.42	3.29	3.56	5.10	5.04	5.28	3.8	29.0
SIMeddy-5d	7	197	3.41	3.27	3.54	5.15	5.08	5.34	3.9	29.3
SIMeddy-5d-clim	7	201	3.28	3.17	3.40	5.15	5.09	5.36	4.0	28.6
SIMeddy-1m	7	145	2.99	2.86	3.10	4.35	4.26	4.55	4.4	29.6
SIMnoeddy-5d	7	53	1.39	1.32	1.46	2.08	2.00	2.08	6.4	23.7
SIMpareddy-5d	6	6	0.28	0.27	0.29	0.31	0.31	0.33	6.2	10.3

Table 3: Summary of spatial mean pseudo-Eulerian and Lagrangian statistics for the greater Agulhas system obtained from surface drifter data (OBS) and the 6 Lagrangian experiments performed in this study: near-surface pseudo-Eulerian mean speed and eddy kinetic energy (EKE), as well as asymptotic (K_{inf}) and maximum (K_{max}) near-surface lateral eddy diffusivity, and Lagrangian integral time (T_L) and length (L_L) scales. The spatial mean has been calculated by averaging over all 416 spatial bins.

Figure caption list

Figure 1: Eulerian fields simulated with the eddy-resolving ocean model configuration INALT01-KJD308. a) Snapshot of the daily mean current speed at 15m depth (15-Jan-2005); b) Long-term mean (1996-2006) Eulerian velocity speed (color shading) and direction (vectors), velocity vectors for speeds > 50 cm s^{-1} are displayed thick and at half-length compared to vectors for speeds < 50 cm s^{-1}; c) Long-term mean (1996-2006) Eulerian EKE, contours are displayed for 50, 100, 300, 700, and 1300 cm^2 s^{-2}. In all subplots, the red dashed frame surrounds the region in which virtual fluid particles were released. The black dashed and solid frames enclose the 5° x 5° and 2° x 2° bins used for the diffusivity calculations and plotting, respectively, for the Agulhas Current (AC), Agulhas Retroflection (AR), Agulhas Return Current (ARC), and eastern South Atlantic Gyre (eSAG).

Figure 2: Time lag dependent near-surface eddy dispersion and diffusivity estimates for the four regions marked in Figure 1, obtained from Lagrangian experiment SIMeddy-5d. a-d) Zonal (s_{xx}, dark blue line), meridional (s_{yy}, light blue line), and minor principal component (s_{p2}, black dashed line) of the ensemble mean single-particle dispersion tensor; e-f) Minor principal component of the half growth rate of the single-particle dispersion tensor (k_{p2}^{disp}, black dashed lines), minor principal component of the symmetric part of the Davis diffusivity tensor (k_{p2}^{davis}, black dotted lines), and combined lateral eddy diffusivity estimate defined as the semi-sum of the two diffusivity measures (K, black solid lines). Red horizontal lines indicate the asymptotic lateral eddy diffusivity estimate (K_{inf}) inferred as the average of K in the red shaded time lag interval 15days ≤ t ≤ 20days. Please note the different scaling of the y-axis in all subplots.

Figure 3: Spatial pattern of asymptotic near-surface eddy diffusivity estimates. Shown are results obtained from Lagrangian experiment SIMeddy-5d (upper panels), and drifter data (OBS, middle panels), as well as the relative difference between simulations and observations (lower panels). Asymptotic eddy diffusivity estimates from a-c) the minor principal component of the half growth rate of the single-particle dispersion tensor K_{inf}^{disp}; d-f) the minor principal component of the symmetric part of the Davis diffusivity tensor K_{inf}^{dav}; and g-i) the combined lateral eddy diffusivity estimate K_{inf}. The relative difference is defined as [SIMeddy-5d – OBS]/OBS, respective contours are displayed at a distance of 0.5.

Figure 4: Spatial pattern of maximum eddy diffusivity estimates and the relation of maximum to asymptotic eddy diffusivity estimates. Shown are results for the combined lateral eddy diffusivity estimates obtained from Lagrangian experiment SIMeddy-5d (upper panels), drifter data (OBS, middle panels), as well as the relative difference between simulations and observations (lower panels). a-c) Maximum eddy diffusivity estimate K_{max}, included here as an approximate measure for the unsuppressed diffusivities; d-f) Relation of K_{max} to the sought-after asymptotic diffusivity estimate K_{inf}, quantifying the strength of eddy diffusivity suppression (color shading), and pseudo-Eulerian mean velocity (vectors, cf. Figure 6). The relative difference is defined as [SIMeddy-5d – OBS]/OBS, respective contours are displayed at a distance of 0.5.

Figure 5: Near-surface pseudo-Eulerian mean velocity and EKE. Shown are results obtained from experiment SIMeddy-5d (upper panels) and drifter data (OBS, middle panels). a-b) Mean speed (contours and color shading), and direction (vectors) of the pseudo-Eulerian mean velocity. Contours are displayed every 5 cm s^{-1}, velocity vectors for speeds > 10 cm s^{-1} are displayed thick and at half-length compared to vectors for speeds < 10 cm s^{-1}. c-d) Pseudo-Eulerian EKE, contours are displayed for 50, 100, 300, 700, and 1300 cm^2 s^{-2}. e-f)

Relative difference defined as [SIMeddy-5d – OBS]/OBS, contours are displayed at a distance of 0.5.

Figure 6: Sensitivity of the asymptotic eddy diffusivity estimates (K_{inf}) to OGCM choices. Shown are results for the combined lateral eddy diffusivity estimates obtained from the Lagrangian experiments performed with the eddy-resolving OGCM configuration INALT01 a) forced with climatological atmospheric fields (SIMeddy-5d-clim), and b) forced with interannually varying atmospheric fields, but using monthly mean velocites (SIMeddy-1m). Also shown are the results from the Lagrangian experiments performed with the non-eddying OGCM configuration ORCA05 c) without (SIMnoeddy-5d), and d) with GM parametrization of baroclinic eddies (SIMpareddy-5d).

Figure 7: Boxplots of the spatial distributions of a) the asymptotic eddy diffusivity estimates K_{inf} and b) pseudo-Eulerian mean EKE. Shown are results for all Lagrangian experiments employed in this study, whereby Kinf was inferred from the combined lateral eddy diffusivity estimate. On each box, the central mark indicates the median calculated out of the 416 overlapping 5° x 5° spatial ocean bins for the greater Agulhas system, the left and right edges of the box indicate the 25th and 75th percentiles, respectively, and the whiskers extend to the minimum and maximum values. The dashed vertical lines indicate the mean values (cf. Table 3).

Figure 8: Lateral eddy diffusivity estimation following Oh et al. (2000).

Figure 9: Robustness of the asymptotic eddy diffusivity estimates (K_{inf}) with respect to smoothing choices. Shown are the results for the combined lateral eddy diffusivity estimates obtained from Lagrangian experiment SIMeddy-5d with different bin sizes and filters

employed: a) overlapping 5° x 5° bins and time-dependent filtering of the diffusivity and dispersion tensors, as well as time-dependent finite differencing as described in the method section (same as Figure 2g); b) overlapping 5° x 5° bins, but no filtering and no time-dependent finite differencing; c) time-dependent filtering of the diffusivity and dispersion tensors, as well as time-dependent finite differencing as described in the method section, but non-overlapping 2° x 2° bins ; d) non-overlapping 2° x 2° bins, as well as no filtering and no time-dependent finite differencing.

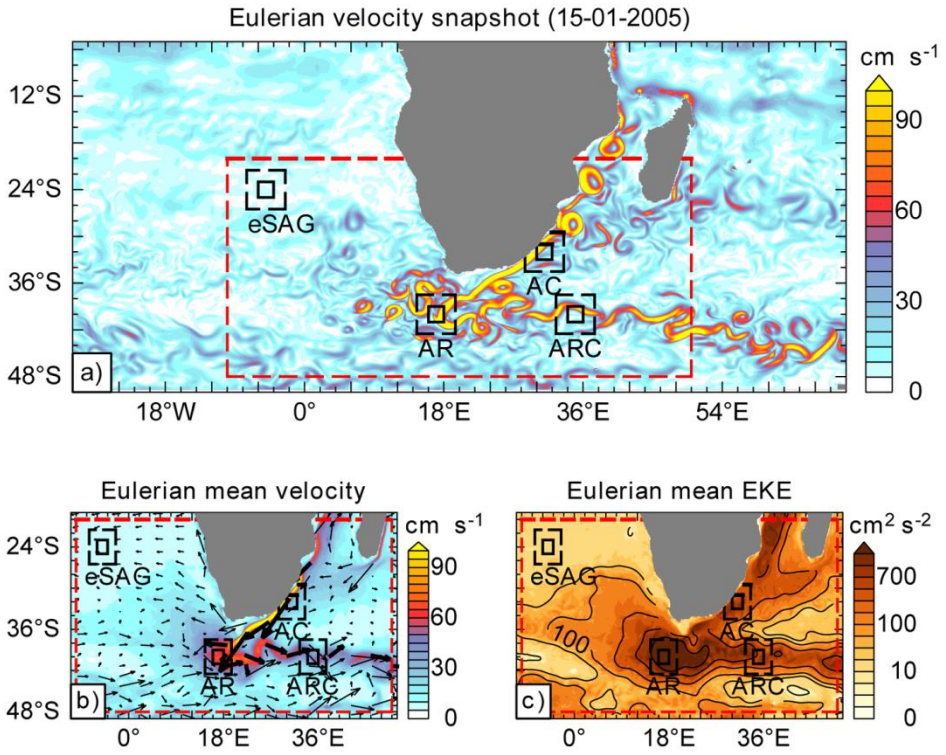

Figure 1: Eulerian fields simulated with the eddy-resolving ocean model configuration INALT01-KJD308. a) Snapshot of the daily mean current speed at 15m depth (15-Jan-2005); b) Long-term mean (1996-2006) Eulerian velocity speed (color shading) and direction (vectors), velocity vectors for speeds > 50 cm s^{-1} are displayed thick and at half-length compared to vectors for speeds < 50 cm s^{-1}; c) Long-term mean (1996-2006) Eulerian EKE, contours are displayed for 50, 100, 300, 700, and 1300 cm^2 s^{-2}. In all subplots, the red dashed frame surrounds the region in which virtual fluid particles were released. The black dashed and solid frames enclose the 5° x 5° and 2° x 2° bins used for the diffusivity calculations and plotting, respectively, for the Agulhas Current (AC), Agulhas Retroflection (AR), Agulhas Return Current (ARC), and eastern South Atlantic Gyre (eSAG).

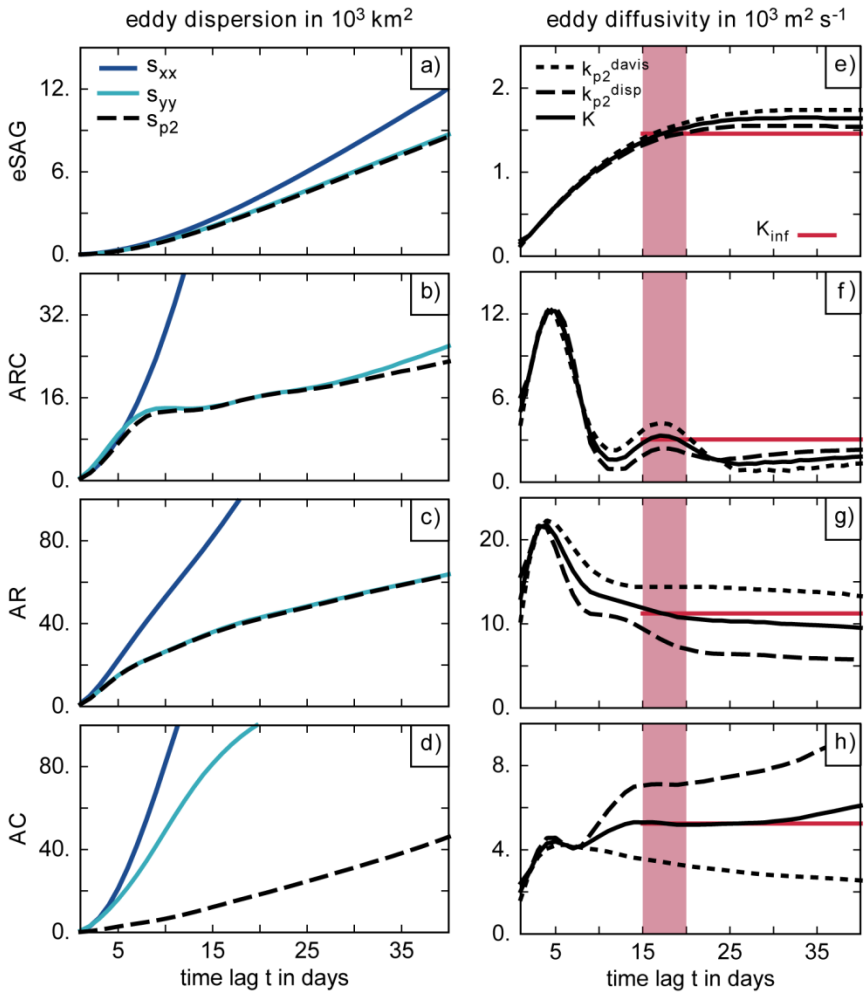

Figure 2: Time lag dependent near-surface eddy dispersion and diffusivity estimates for the four regions marked in Figure 1, obtained from Lagrangian experiment SIMeddy-5d. a-d) Zonal (s_{xx}, dark blue line), meridional (s_{yy}, light blue line), and minor principal component (s_{p2}, black dashed line) of the ensemble mean single-particle dispersion tensor; e-f) Minor principal component of the half growth rate of the single-particle dispersion tensor (k_{p2}^{disp}, black dashed lines), minor principal component of the symmetric part of the Davis diffusivity tensor (k_{p2}^{davis}, black dotted lines), and combined lateral eddy diffusivity estimate defined as the semi-sum of the two diffusivity measures (K, black solid lines). Red horizontal lines indicate the asymptotic lateral eddy diffusivity estimate (K_{inf}) inferred as the average of K in the red shaded time lag interval 15days ≤ t ≤ 20days. Please note the different scaling of the y-axis in all subplots.

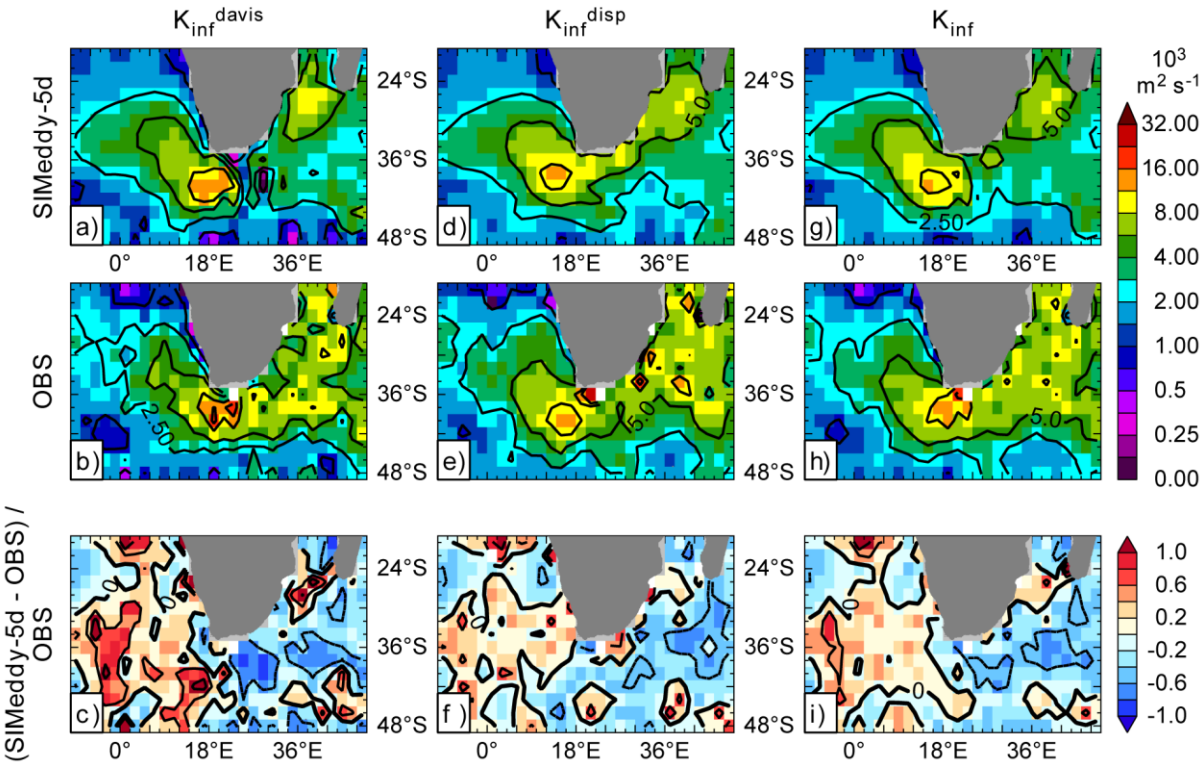

1172

1173 **Figure 3: Spatial pattern of asymptotic near-surface eddy diffusivity estimates.** Shown
1174 are results obtained from Lagrangian experiment SIMeddy-5d (upper panels), and drifter data
1175 (OBS, middle panels), as well as the relative difference between simulations and observations
1176 (lower panels). Asymptotic eddy diffusivity estimates from a-c) the minor principal
1177 component of the half growth rate of the single-particle dispersion tensor K_{inf}^{disp}; d-f) the
1178 minor principal component of the symmetric part of the Davis diffusivity tensor K_{inf}^{dav}; and g-
1179 i) the combined lateral eddy diffusivity estimate K_{inf}. The relative difference is defined as
1180 [SIMeddy-5d – OBS]/OBS, respective contours are displayed at a distance of 0.5.

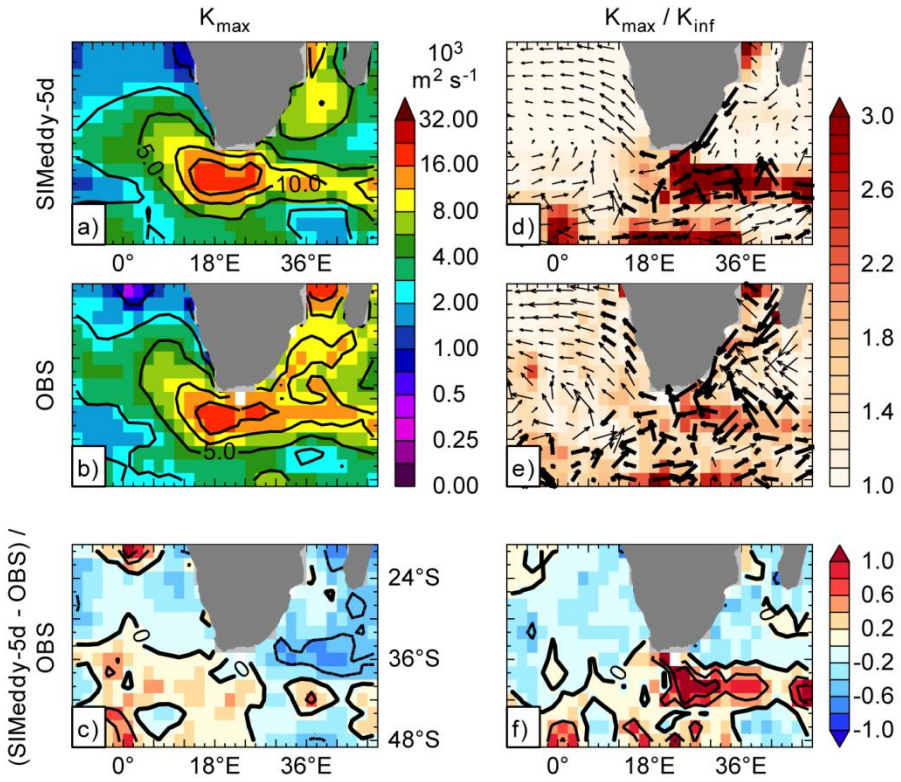

Figure 4: Spatial pattern of maximum eddy diffusivity estimates and the relation of maximum to asymptotic eddy diffusivity estimates. Shown are results for the combined lateral eddy diffusivity estimates obtained from Lagrangian experiment SIMeddy-5d (upper panels), drifter data (OBS, middle panels), as well as the relative difference between simulations and observations (lower panels). a-c) Maximum eddy diffusivity estimate K_{max}, included here as an approximate measure for the unsuppressed diffusivities; d-f) Relation of K_{max} to the sought-after asymptotic diffusivity estimate K_{inf}, quantifying the strength of eddy diffusivity suppression (color shading), and pseudo-Eulerian mean velocity (vectors, cf. Figure 6). The relative difference is defined as [SIMeddy-5d – OBS]/OBS, respective contours are displayed at a distance of 0.5.

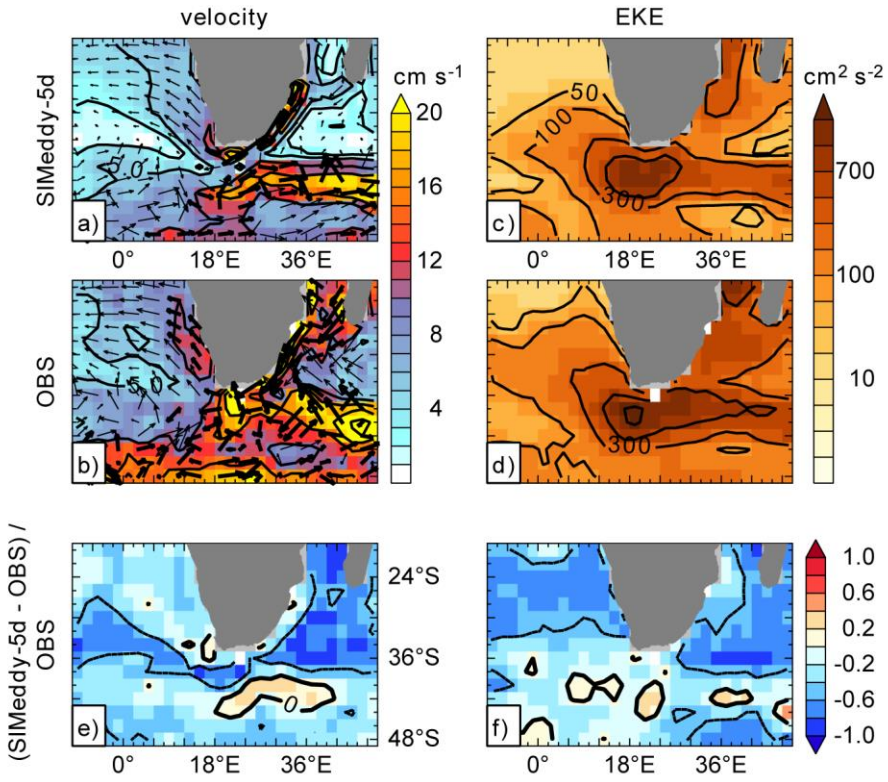

1192

1193 **Figure 5: Near-surface pseudo-Eulerian mean velocity and EKE.** Shown are results

1194 obtained from experiment SIMeddy-5d (upper panels) and drifter data (OBS, middle panels).

1195 a-b) Mean speed (contours and color shading), and direction (vectors) of the pseudo-Eulerian

1196 mean velocity. Contours are displayed every 5 cm s^{-1}, velocity vectors for speeds > 10 cm s^{-1}

1197 are displayed thick and at half-length compared to vectors for speeds < 10 cm s^{-1}. c-d)

1198 Pseudo-Eulerian EKE, contours are displayed for 50, 100, 300, 700, and 1300 cm^2 s^{-2}. e-f)

1199 Relative difference defined as [SIMeddy-5d – OBS]/OBS, contours are displayed at a

1200 distance of 0.5.

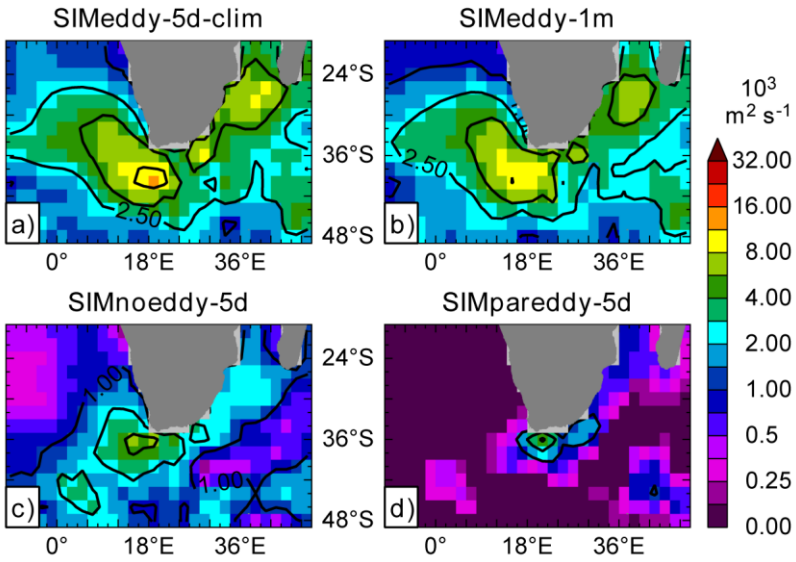

Figure 6: Sensitivity of the asymptotic eddy diffusivity estimates (K_{inf}) to OGCM choices. Shown are results for the combined lateral eddy diffusivity estimates obtained from the Lagrangian experiments performed with the eddy-resolving OGCM configuration INALT01 a) forced with climatological atmospheric fields (SIMeddy-5d-clim), and b) forced with interannually varying atmospheric fields, but using monthly mean velocites (SIMeddy-1m). Also shown are the results from the Lagrangian experiments performed with the non-eddying OGCM configuration ORCA05 c) without (SIMnoeddy-5d), and d) with GM parametrization of baroclinic eddies (SIMpareddy-5d).

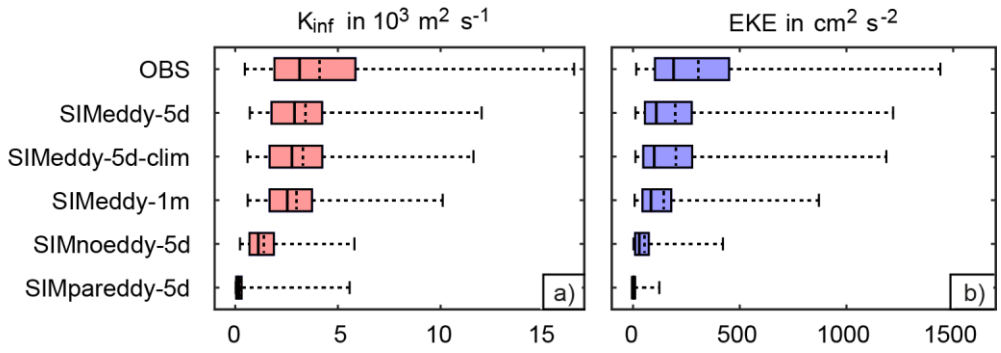

Figure 7: Boxplots of the spatial distributions of a) the asymptotic eddy diffusivity estimates K_{inf} and b) pseudo-Eulerian EKE. Shown are results for all Lagrangian experiments employed in this study, whereby Kinf was inferred from the combined lateral eddy diffusivity estimate. On each box, the central mark indicates the median calculated out of the 416 overlapping 5° x 5° spatial ocean bins for the greater Agulhas system, the left and right edges of the box indicate the 25th and 75th percentiles, respectively, and the whiskers extend to the minimum and maximum values. The dashed vertical lines indicate the mean values (cf. Table 3).

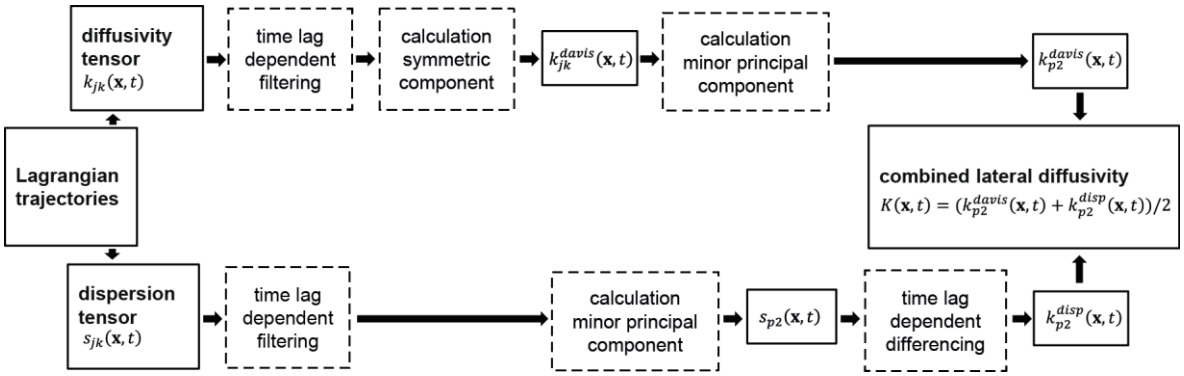

Figure 8: Lateral eddy diffusivity estimation following Oh et al. (2000).

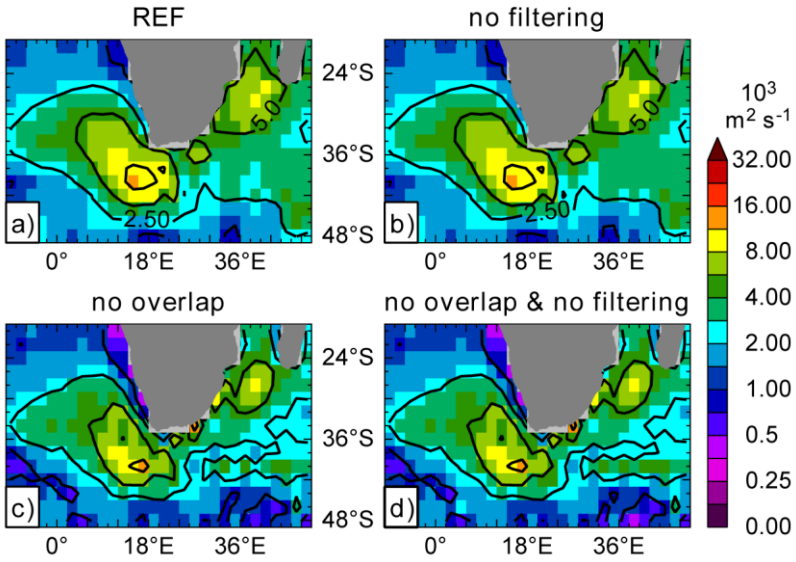

Figure 9: Robustness of the asymptotic eddy diffusivity estimates (K_{inf}) with respect to smoothing choices. Shown are the results for the combined lateral eddy diffusivity estimates obtained from Lagrangian experiment SIMeddy-5d with different bin sizes and filters employed: a) overlapping 5° x 5° bins and time-dependent filtering of the diffusivity and dispersion tensors, as well as time-dependent finite differencing as described in the method section (same as Figure 2g); b) overlapping 5° x 5° bins, but no filtering and no time-dependent finite differencing; c) time-dependent filtering of the diffusivity and dispersion tensors, as well as time-dependent finite differencing as described in the method section, but non-overlapping 2° x 2° bins ; d) non-overlapping 2° x 2° bins, as well as no filtering and no time-dependent finite differencing.